Quantum phases, Supersolids and quantum phase transitions of interacting bosons in frustrated lattices

Yan Chen [1] and Jinwu Ye [2]
[1] *Department of Physics, Surface Physics Laboratory (National Key Laboratory) and Lab of Advanced Materials, Fudan University, Shanghai, China*
[2] *Department of Physics, The Pennsylvania State University, University Park, PA, 16802*
(Dated: May 4, 2010)

By using the dual vortex method (DVM), we study some phases and phase transitions in an extended boson Hubbard model slightly away from 1/3 (2/3) filling on frustrated lattices such as triangular and kagome lattice. We develop systematically a simple and effective way to use the vortex degree of freedoms on dual lattices to characterize the symmetry breaking patterns of the boson insulating states in the direct lattices. In the triangular lattice at 1/3, we find a X-CDW, a stripe CDW phase which was found perviously by a density operator formalism (DOF). Most importantly, we also find a new CDW-VB phase which has both local CDW and local VB orders, in sharp contrast to a bubble CDW phase found previously by the DOF. In the Kagome lattice at 1/3, we find a VBS phase and a 6 fold-CDW phase. Most importantly, we also find the CDW-VB phase which has both local CDW and local VB orders which was found in previous QMC simulations. We also study several other phases which are not found by the DVM. By analyzing carefully the saddle point structures of the dual gauge fields in the translational symmetry breaking side, we find that the CDW to SF transition in the triangular is likely to be a strong first order one, while the CDW+VB to the SF transition in Kagome lattice is likely to be a weakly first order one. This findings by the DVM can give some explanations to some puzzles observed in the QMC in both lattices. Then by pushing the effective actions slightly away from the commensurate filling $f = 1/3$, we classified all the possible types of supersolids and analyze their stability conditions. In a triangular lattice, there are X-CDW supersolid, stripe CDW supersolid, but absence of any valence bond supersolid (VB-SS). There are also a new kind of supersolid: CDW-VB supersolid. In a Kagome lattice, there are 6 fold-CDW supersolid, stripe CDW supersolid, but absence of any valence bond supersolid (VB-SS). There are also a new kind of supersolid: CDW-VB supersolid. We show that independent of the types of the SS, the quantum phase transitions from solids to supersolids driven by a chemical potential are in the same universality class as that from a Mott insulator to a superfluid, therefore have exact exponents $z = 2, \nu = 1/2, \eta = 0$ (with logarithmic corrections). Implications on QMC simulations with both nearest neighbor and next nearest neighbor interactions in both lattices are given. Some possible problems of the DOF in identifying the insulating phases are also pointed out.

I. INTRODUCTION

The EBHM with various kinds of interactions, at various kinds lattices (bi-partisan or frustrated) at various kinds of filling factors (commensurate or in-commensurate) is described by the following Hamiltonian[1–3]:

$$H = -t \sum_{<ij>} (b_i^\dagger b_j + h.c.) - \mu \sum_i n_i + \frac{U}{2} \sum_i n_i(n_i - 1) + V_1 \sum_{<ij>} n_i n_j + V_2 \sum_{<<ik>>} n_i n_k + \cdots \quad (1)$$

where $n_i = b_i^\dagger b_i$ is the boson density, t is the hopping amplitude, U, V_1, V_2 are onsite, nearest neighbor (nn) and next nearest neighbor (nnn) interactions between the bosons. The $\cdots$ may include further neighbor interactions and possible ring-exchange interactions. A supersolid in Eqn.1 is defined as to have both off-diagonal long range order $< b_i > \neq 0$ and diagonal charge density wave in the boson density n_i which break the lattice symmetry. In frustrated lattices, the sign of the hopping t in Eqn.1 makes the crucial difference[2]. This difference leads to many new and interesting physics in frustrated lattices which are quite different than those in bipartite lattices studied in[1,4,5].

In cold atom experiments[6,7], the on-site interaction U can be tuned by the Feshbach resonance. Various kinds of optical lattices can be realized by suitably choosing the geometry of the laser beams forming the optical lattices. For example, using three coplanar beams of equal intensity having the three vectors making a 120° angle with each other[8], the potential wells have their minima in a honeycomb or a triangular lattice. Four beams travel along the three fold symmetry axes of a regular tetrahedron, the potential wells have their minima in a body-centered-cubic lattice[8]. The authors in[9] proposed to create a kagome optical lattice using superlattice techniques. There are many possible ways to generate longer range interaction $V_1, V_2, ...$ of ultra-cold atoms loaded in optical lattices (1) Very exciting perspectives have been opened by recent experiments on cooling and trapping of ^{52}Cr atoms[10] and fermionic polar molecules $^{40}K+^{87}Rb$[11]. The bosonic polar molecules $^{39}K+^{87}Rb$ is also expected in near future. Being magnetically or electrically polarized, the ^{52}Cr atoms or polar molecules interact with each other via long-rang anisotropic dipole-dipole interactions. Loading the ^{52}Cr or the polar molecules on a 2d

optical lattice with the dipole moments perpendicular to the trapping plane can be mapped to Eqn.1 with long-range repulsive interactions $\sim p^2/r^3$ where p is the dipole moment. The CDW supersolid phases described by the dual vortex method (DVM) in[5] was numerically found to be stable in large parameter regimes in this system[12]. Possible techniques to generate long-range interactions in a gas of groundstate alkali atoms by weakly admixing excited Rydberg states[13] with laser light was proposed in[14]. Very recently, the cold bosons or fermions in optical lattice can interact with a very long range interaction due to the exchange of cavity photons[15]. The generation of the ring exchange interaction has been discussed in[16].

From a spin wave $1/S$ expansion, the authors in[2] found that a SS state is more robust in a triangular lattice with only t and V_1 terms in Eqn.1 and a SS state with $\sqrt{3} \times \sqrt{3}$ pattern is stable even at half filling $f = 1/2$. Indeed, this discovery was confirmed by several recent QMC simulations in the EBHM of hard core bosons with the nearest neighbor (NN) interaction[17–20]. However, due to too strong quantum fluctuations, the authors in[2] found that the spin wave expansion does not work anymore in Kagome lattice. So a different analytical method is needed to study possible supersolid phases in a Kagome lattice.

Recently, the EBHM in a square lattice at generic commensurate filling factors $f = p/q$ (p, q are relative prime numbers) were systematically studied in[1] by a dual vortex method (DVM). The DVM method was applied by one of the authors to study the EBHM on bipartite lattices such as honeycome and square lattice at half and near half fillings and its possible experimental applications in cold atoms, adatom absorptions on substrates and possible Cooper-pair supersolids in high temperature superconductors. It was pointed out in[5] that the DVM developed in[1] holds in the superfluid (SF) and the valence bond solid (VBS) side where the saddle point of the dual gauge field can be taken as uniform, but cares are needed to apply the DVM developed in[1] in the CDW side where the saddle point of the dual gauge field can *not* be taken as uniform anymore. When studying phases and phase traditions slightly away from 1/2 filling, special care is needed to choose a correct saddle point of the dual gauge field in the CDW side, so a different effective action is needed in the CDW side to make the theory self-consistent[5]. In[5], (1) by extending the DVM explicitly to the lattice symmetry breaking side by choosing the corresponding self-consistent saddle points of the dual gauge field (2) by pushing the DVM to slightly away from commensurate filling factors, the author mapped out the global phase diagram at $T = 0$ of the chemical potential versus the ratio of the kinetic energy over the interaction. It was found that in the insulating side, different kinds of supersolids are generic possible states slightly away from half filling. A novel kind of supersolid called valence bond supersolid (VB-SS) was proposed. It was also shown that the transition from a CDW (Valence bond) solid to a CDW (valence bond) supersolid driven by the chemical potential is in the same universality class as the Mott to the SF with the exact exponents $z = 2, \nu = 1/2, \eta = 0$ subject to a logarithmic correction. It was also suggested that the density order parameter constructed in[1] to characterize the symmetry breaking patterns in the insulating states are also not physically transparent. It is very hard to generalize the density operator to a honeycomb lattice and other lattices. The subsequent QMC simulations on the EBHM of hard and soft core bosons with the nearest neighbor (NN) interaction on a honeycomb lattice[24] indeed found a stable X-supersolid phase in the soft core case slightly above the half filling.

The DVM method was extended to study the EBHM in a triangular lattice at 1/3 and 1/2 fillings in[21]. Starting from the SF side, the authors derived the effective action Eqn.3 to describe quantum phase transitions from the SF to some insulating states with several kinds of lattice symmetry breaking patterns. By generalizing the density operators in the square lattice constructed in[1] to those in a triangular lattice, they identified an X-solid phase at $f = 1/3$ in the Ising limit of the effective action, a stripe solid phase and a bubble solid phase in two possible easy plane limits. They suggested that the transition from the SF to the stripe solid could be second order through the so-called de-confined quantum critical point[22]. Then subsequent QMC simulations on the EBHM Eqn.12 of hard core bosons with a next nearest neighbor (NNN) interaction in[23] indeed found the stripe solid phase as a ground state at $f = 1/3$ in some parameter regimes. The QMC in[23] seems also to find a meta-stable bubble phase which has higher energy than the stripe phase in the same parameter regimes. However, they found the transition from the SF to the stripe solid phase at $f = 1/3$ is a strong first order transition. Later, the DVM was applied to study the EBHM on a Kagome lattice in[25]. From the Magnetic space group (MSG), starting from the SF side, the authors derived the effective action Eqn.3 to describe quantum phase transitions from the SF to some insulating states with some lattice symmetry breaking patterns. Realizing it is not convenient to generalize the density operators in the square lattice constructed in[1] to the Kagome lattice, they tied to use the vortex fields on the dual dice lattice to identify possible symmetry breaking patterns in the insulating side. Unfortunately, because the vortex fields are gauge dependent, so may not be used to characterize symmetry breaking patterns effectively. There are also two QMC simulations on the EBHM of hard core bosons with nearest neighbor (NN) interaction in a Kagome lattice[26,27]. Both groups found that the solid state at $f = 1/3$ has both CDW and VB order. The VB order corresponds to boson hopping around a hexagon (see Fig.13b). However, they did not see any stable supersolid phase away from the 1/3 filling in the hard core case. Although the QMC in Ref.[27] suggested that the the SF to the CDW+VB solid transition is a 2nd order transition through the deconfined quantum critical point[22], the QMC in Ref.[26] concluded a weakly 1st order

transition from a double-peaked histogram of the boson kinetic energy.

In this paper, we will use the DVM developed in[1,4,5] to study quantum phases, especially various kinds of insulating phases and phase transitions in the two most common frustrated lattices such as triangular and kagome lattices at and slightly away 1/3 and 2/3 fillings. We contrast different symmetry breaking patterns of the insulating phases in both Ising and Easy plane limits in the two lattices. We will also compare our results with some previous Quantum Monte-Carlo (QMC) results in the two lattices[23,26] and also give important implications to possible future QMC simulations on the EBHM Eqn.1 with both hard and soft cores, with both the NN V_1 and the NNN V_2 interactions. We develop a systematic way to determine the symmetry breaking patterns of the insulating states in terms of the vortex degree of freedoms only at the dual lattice points. These vortex degree of freedoms are the gauge invariant physical vortex densities, the kinetic energies and vortex currents defined in Eqn.7,8. In the triangular lattice, we found the X-solid phase in the Ising limit $v > 0$, the stripe phase in one of the easy plane limit $v < 0, w < 0$, both of which were found before by the density operator formalism in[21]. However, we identify a novel phase with both CDW and VB orders shown in Fig.7 in another easy plane limit $v < 0, w > 0$. This finding differs from the bubble solid phase shown in Fig.25 in the same easy plane limit found by the density operator formalism in[21]. This disagreement calls for the reexamination of the correctness and effectiveness of the density operator formalism in terms of the dual vortex degree of freedoms in general lattices at general filling factors. The quantum phases and phase transitions in a Kagome lattice in both Ising and easy plane limit are dramatically different from those in bipartite[1,4,5] and triangular lattice studied previously[21] and in the Sec.II. So far, the density operator formalism in[5,21] has not been generalized to the Kagome lattice However, by using our method, we identify a triangular valence bond (TVB) solid phase in the Ising limit $v > 0$, a 6-fold CDW phase in one of the easy plane limit $v < 0, w < 0$, the CDW-VB phase first discovered in the QMC in[26,27] in the other easy plane limit $v < 0, w > 0$. In fact, this 6-fold CDW phase has the same symmetry breaking patterns as the CDW-VB phase, however, the crucial difference is that the former has a local CDW order, while the latter has a local VBS order. In the Ising limit, the SF to the triangle valence bond order (TVB) is a weak first order one. For the first time, the Ising limit of the same action can be used to describe a VBS phase in a concrete model. In the easy-plane limit, we find that the 6 fold CDW to the SF transition, also the CDW+VB to the SF transition at commensurate filling $f = 1/3$ in Kagome lattice are a weakly first order one. This finding resolves some outstanding puzzles observed in the QMC in a kagome lattice[26,27]. The firm identification of this CDW-VB phase in the easy-plane limit $v < 0, w > 0$ is important, because one is sure that the effective action Eqn.13 in terms of the two vortex fields ϕ_0, ϕ_1 in the easy-plane limit $v < 0, w > 0$ indeed describes the SF to the CDW-VB transition studied by the QMC[26,27] in a simple microscopic EBHM Eqn.11 in a Kagome lattice. This EBHM Eqn.11 is very simple and has no ring exchange interaction which is usually needed to stabilize a VBS order in a bipartite lattice. The results in[26] showed that this transition is a very weak first order one instead of a second order one through the DCQCP. We also study briefly the excitation spectra in these insulating phases. It is interesting to note that one can achieve different CDW+VB states in the easy plane limit $v < 0, w > 0$ in both triangular and Kagome lattices from the DVM. The method developed here should be very general and can be used to characterize uniquely the symmetry breaking patterns in any lattices at any filling factors by using the vortex degree of freedoms only at the corresponding dual lattice points.

Then we study possible quantum phases and quantum phase transitions slightly away from 1/3(2/3) fillings in the two frustrated lattices. When pushing the effective action slightly away from the commensurate fillings inside various insulating phases, we find that one has to choose the corresponding saddle point structure of the dual gauge field carefully and self-consistently to construct the effective actions away from the commensurate fillings on insulating side. We classified all the possible types of supersolids (SS) and analyze their stability conditions. In a triangular lattice, there are X-CDW SS and stripe CDW SS which are stable in both hard core and soft core cases, but absence of any Valence bond supersolid (VB-SS). There are also a new kind of supersolid: CDW-VB supersolid which maybe stable only in the soft core case. This novel kind of supersolid has CDW, VBS and superfluid order. The supersolid in the triangular lattice near 1/2 filling can be considered as doping the adjacent solid at 1/3 filling by interstitials (SS-i in Fig.9) or as doping the adjacent solid at 2/3 filling by vacancies (SS-v in Fig.9). The supersolid at exactly 1/2 is the coexistence of SS-i and SS-v with any possible ratio. *There are only two kinds of supersolids: vacancy type or interstitial type. There is no other kinds of supersolids.* The 1/2 filling at triangular lattice may not be a " commensurate " filling as thought previously. Only 1/3(2/3) are commensurate fillings. Therefore the SS in triangular lattice has the same origin as that in the square lattice discussed in[5]. In a Kagome lattice in the Ising limit, there can only be a direct first-order transition from the triangular valence bond (TVB) to the SF, so there is no immediate TVB supersolid intervening between the TVB and the SF. However, in the Easy-plane limit, different kinds of supersolids are generic states slightly away from 1/3 (2/3) filling. In addition to a 6-fold CDW supersolid, the stripe supersolid (stripe-SS), we also find a new kind of supersolid: CDW-VB supersolid. The stripe-SS should be stable even in the hard core limit, while the stripe-SS and CDW-VB-SS maybe stable only in the soft core limit. The absence of the VB-SS in frustrated lat-

tices is in sharp contrast to that in bipartite lattices discovered in[4,5]. The quantum phase transitions from solids to the adjacent supersolids (if they exist) driven by a chemical potential are in the same universality class as that from a Mott insulator to a superfluid, therefore have exact exponents $z = 2, \nu = 1/2, \eta = 0$ (with logarithmic corrections). The superfluid density in the SS scales as $\rho_s \sim |\rho - 1/3|^{(d+z-2)\nu} = |\rho - 1/3| = \delta f$ with logarithmic corrections. In the anisotropic stripe SS case, the superfluid densities along different directions should scale the same way with different coefficients. We also made implications on the available and future QMC simulations on EBHM with both NN and NNN interactions in both lattices.

The rest of the paper are organized as follows. In the section II, we study the EBHM in a triangular lattice. We first outline the method to characterize the symmetry breaking patterns in the insulating side using the vortex degree of freedoms only at dual lattice sides. Then we identify the X-CDW phase in the Ising limit in Sec.II-A, the stripe CDW phase in Sect.II-B-1, the new and the most interesting CDW-VB solid phase in Sect.II-B-2, the VBS phase in Sect.II-C, then compare with QMC in Sec.II-D. We also construct effective actions to study possible supersolid phases and their stabilities slightly away from the 1/3 filling. In the section III, we study the EBHM in a Kagome lattice. We identify the VBS phase in the Ising limit in Sec.III-A, the most interesting CDW-VB phase in Sect.III-B-1, the 6 fold CDW phase in Sect.III-B-2, the stripe CDW phase in Sect.III-C, then compare with QMC in Sec.III-D. We also construct effective actions to study possible supersolid phases and their stabilities slightly away from the 1/3 filling. We summarize our results and give some perspectives on comparing the DVM and the QMC simulations in the concluding Sect.IV. In the appendix A and B, we use the same method to identify insulating phases in square lattice and honeycomb lattice respectively, also the excitation spectra in all these phases. In appendix C, we compare our method with the density wave operator formalism used in[1,21] and commented on possible weakness of the formalism. In appendix C, we list specific vortex fields values used in Sect. II-B-2 for the CDW-VB phase. A very short version in the part of Kagome lattice appeared in a unpublished preprint[28].

II. SOLID AND SUPERSOLID NEAR 1/3(2/3) ON TRIANGULAR LATTICE

Triangular lattice is the simplest frustrated lattice (Fig.1a). From spin wave expansion, the authors in[2] found that a SS state is more robust in a triangular lattice with only t and V_1 terms in Eqn.1 and a SS state with $\sqrt{3} \times \sqrt{3}$ pattern is stable even at half filling $q = 2$. Indeed, this discovery was confirmed by several recent QMC simulations[17–20].

We will investigate the phases and quantum phase transitions when slightly away from the 1/3 filling. Because of the P-H symmetry at $U = \infty$, the results are equally valid near 2/3 filling. As shown in the Table 1 in[3], for $q = 3$, there are 3 minima at $(0,0), (0, 2\pi/3), (0, 4\pi/3)$. Let's label the three eigenmodes at the three minima as $\xi_l, l = 1, 2, 3$. The general effective action in terms of the three modes invariant under all the MSG transformations upto sixth order terms was written down[21]. The effective action can be simplified in the permutative representation basis $\phi_l, l = 1, 2, 3$ given by:

$$\begin{aligned} \xi_0 &= \frac{1}{\sqrt{3}}(\phi_0 + e^{i\frac{2\pi}{3}}\phi_1 + \phi_2) \\ \xi_1 &= \frac{1}{\sqrt{3}}(e^{i\frac{2\pi}{3}}\phi_0 + \phi_1 + \phi_2) \\ \xi_2 &= \frac{1}{\sqrt{3}}(\phi_0 + \phi_1 + e^{i\frac{2\pi}{3}}\phi_2) \end{aligned} \quad (2)$$

In the superfluid side, moving *slightly* away from the 1/3 filling $f = 1/3$ corresponds to adding a small *mean* dual magnetic field $\delta f = f - 1/3$ in the action derived in[21]. Upto sixth order, the action is $\mathcal{L}_{SF} = \mathcal{L}_0 + \mathcal{L}_1 + \mathcal{L}_2$:

$$\begin{aligned} \mathcal{L}_0 &= \sum_l |(\partial_\mu - iA_\mu)\phi_l|^2 + r|\phi_l|^2 + (\epsilon_{\mu\nu\lambda}\partial_\nu A_\lambda - 2\pi\delta f \delta_{\mu\tau})^2/4 \\ \mathcal{L}_1 &= u(|\phi_0|^2 + |\phi_1|^2 + |\phi_2|^2)^2 - v[(|\phi_0|^2 - |\phi_1|^2)^2 \\ &+ (|\phi_1|^2 - |\phi_2|^2)^2 + (|\phi_2|^2 - |\phi_0|^2)^2] \\ \mathcal{L}_2 &= w[(\phi_0^*\phi_1)^3 + (\phi_1^*\phi_2)^3 + (\phi_2^*\phi_0)^3 + h.c.] \end{aligned} \quad (3)$$

where A_μ is a non-compact $U(1)$ gauge field.

Because the duality transformation is a non-local transformation, the relations between the phenomenological parameters in Eqn.3 and the microscopic parameters in Eqn.1 are highly non-local and not known. Fortunately, we are still able to classify some phases and phase transitions from Eqn.3 without knowing these relations. If $< \phi_l >= 0$ for every $l = 1, 2, 3$, the system is in the SF state. If $< \phi_l > \neq 0$ for at least one l, the system is in the insulating state.

The Harper's equation in the unit cell chosen in the Fig.4 in[3] was derived in Eqn. A2 in[3]. The authors in Ref.[21] chose a different unit cell in their Fig.1 which is the same as Fig.1. In order to be consistent with the formalism developed in[21], we can derive the Harper's equation at the filling factor $f = 1/q$ corresponding to the unit cell in Fig.1b:

$$\begin{aligned} c^a_{m-1}(k_x, k_y) &+ e^{ik_y}(1 + e^{i(k_x + 2\pi f m)})c^a_m(k_x, k_y) \\ &= \epsilon(k_x, k_y)c^b_m(k_x, k_y), \\ c^b_{m+1}(k_x, k_y) &+ e^{-ik_y}(1 + e^{-i(k_x + 2\pi f m)})c^b_m(k_x, k_y) \\ &= \epsilon(k_x, k_y)c^a_m(k_x, k_y) \end{aligned} \quad (4)$$

where $m = 0, 1, \cdots, q-1$ and a, b are two sublattices of the honeycomb lattice. $-\pi/q \leq k_x \leq \pi/q, -\pi \leq k_y \leq \pi$ are inside the reduced Brillouin zone. The q minima of the $2q$ bands $\epsilon(k_x, k_y)$ was found to at $(k_x, k_y) = (0, 2\pi f l)$.

In the following, we focus on $q = 3$ case. One only need to find the eigenvalues and the corresponding eigenvectors of the 6×6 matrix at the 3 minima $(k_x, k_y) = (0, 2\pi l/3)$ at $l = 0, 1, 2$:

$$A_l = \begin{pmatrix} 0 & 0 & 0 & 2e^{-i2\pi l/3} & 1 & 0 \\ 0 & 0 & 0 & 0 & e^{-i2\pi l/3}(1+e^{-i2\pi/3}) & 1 \\ 0 & 0 & 0 & 1 & 0 & e^{-i2\pi l/3}(1+e^{i2\pi/3}) \\ 2e^{i2\pi l/3} & 0 & 1 & 0 & 0 & 0 \\ 1 & e^{i2\pi l/3}(1+e^{i2\pi/3}) & 0 & 0 & 0 & 0 \\ 0 & 1 & e^{i2\pi l/3}(1+e^{-i2\pi/3}) & 0 & 0 & 0 \end{pmatrix} \quad (5)$$

In fact, we only need the eigenvector $c^a_m(l = 0) = c^a_m, c^b_m(l = 0) = c^b_m$ at $l = 0$. The lowest eigenvalue is $\epsilon = -(1 + 2\cos 2\pi/9)t$, the corresponding eigenvector is $(c^a_m, c^b_m) = [(2\cos 4\pi/9 + 2\cos 2\pi/9 + 1), 1/2 - i\sqrt{3}/2, 2\cos 2\pi/9, (2\cos 4\pi/9 + 2\cos 2\pi/9 + 1), 2\cos 2\pi/9, 1/2 - i\sqrt{3}/2]$. Note that $c^b_0 = c^a_0, c^b_1 = c^a_2, c^b_2 = c^a_1$. The eigen-vectors at $l = 1, 2$ can be achieved by the magnetic translation[1,21] along $\vec{a}_1$: $c^a_m(l) = c^a_m\omega^{-ml}, c^b_m(l) = c^b_m\omega^{-ml}\omega^l$ where $\omega = e^{i2\pi f}$. The eigenfunctions at the three minima $(k_x, k_y) = (0, 2\pi l/3)$ are $\psi^a_l(\vec{x}) = \sum_{m=0}^{q-1} c^a_m(l)e^{i2\pi f(ma_1+la_2)}, \psi^b_l(\vec{x}) = \sum_{m=0}^{q-1} c^b_m(l)e^{i2\pi f(ma_1+la_2)}$ where $\vec{x} = a_1\vec{a_1}+a_2\vec{a_2}$ belongs to the sublattice a and $\vec{x}+\vec{\delta}, \vec{\delta} = 1/3\vec{a_1}+2/3\vec{a_2}$ belongs to the sublattice b. One can write the two component vortex field at $(k_x, k_y) = (0, 2\pi l/3)$ as $\Psi_l(\vec{x}) = (\psi^a_l(\vec{x}), \psi^b_l(\vec{x}))$. Then one can write the total vortex field as the expansion $\Psi(\vec{x}) = \sum_{l=0}^{2} \Psi_l(\vec{x})\xi_l$, namely:

$$\begin{aligned} \psi^a(\vec{x}) &= \sum_{m=0}^{2} c^a_m e^{i2\pi ma_1/3}[\xi_0 + \xi_1\omega^{-m}e^{i2\pi a_2/3} + \xi_2\omega^m e^{-i2\pi a_2/3}] \\ \psi^b(\vec{x}) &= \sum_{m=0}^{2} c^b_m e^{i2\pi ma_1/3}[\xi_0 + \xi_1\omega^{-m+1}e^{i2\pi a_2/3} + \xi_2\omega^{m-1}e^{-i2\pi a_2/3}] \end{aligned} \quad (6)$$

for the vortex fields at sublattice a and sublattice b respectively.

In the Eqn.6, the ξ_0, ξ_1, ξ_2 are determined by the ϕ_0, ϕ_1, ϕ_2 in the permutative representation in Eqn.2. Plugging in the mean field solutions in Sec. II-B, one can determine the vortex fields in the whole dual honeycomb lattice. Therefore, one can extract the corresponding valence bond order in the direct triangular lattice.

The physical quantities can only be the gauge invariant quantities: the densities at different sites in sublattices a and b:

$$|\psi_a(\vec{x})|^2, \qquad |\psi_b(\vec{x})|^2 \quad (7)$$

and the bond quantities between sublattice a and sublattice b :

$$\psi^\dagger_b(\vec{x})e^{i2\pi f a_1}\psi_a(\vec{x}) = K - iI \quad (8)$$

where $\vec{x}$ belongs to the same unit cell shown in Fig.1b. All the other bonds having no phase factor from the gauge field. The real part K gives the kinetic energy between the two sites. The imaginary part I gives the current between the two sites. Note that the "-" sign in Eqn.8 is important which make the definition of the current to be consistent with that of gauge factors in the Fig.1b. $\chi_p = \sum_p I$ around any plaquette p (a hexagon) gives the chirality around the hexagon. The chirality χ_p leads to a boson density at the center of the hexagon p.

A. Ising limit $v > 0$.

If $v > 0$, the system is in the Ising limit, only one of the 3 vortex fields condense. For example, substituting $\phi_0 = 1, \phi_1 = \phi_2 = 0$ into Eqns.2,6,7,8 one can evaluate the vortex densities, kinetic energy and the current in the dual honeycomb lattice. For simplicity, we only show the currents in the Fig.2 which are obviously conserved. By counting the segments of currents along the bonds surrounding the X, Y, Z lattice points, paying special attentions to their counter-clockwise or clock wise directions, we can calculate the densities at these points $n_x = 1/3 + 6xI > 1/3, n_y = n_z = 1/3 - 3xI < 1/3$ where

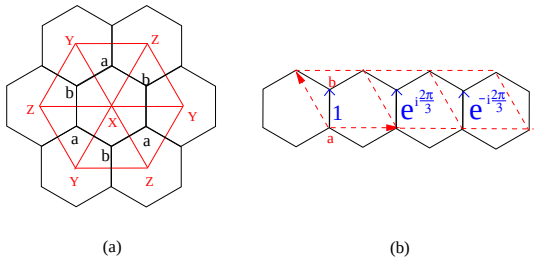

FIG. 1: (a) Bosons at filling factor f are hopping on a triangular lattice (solid line) which has three sublattices X, Y, Z. Its dual lattice is a honeycomb lattice (dashed line) which has two sublattices a and b. (b) The bond phase factors in a dual honeycomb lattice at $f = 1/3$. The direction of the gauge field is important. At $f = 2/3$, the bond phase factors are just complex conjugate of those at $f = 1/3$.

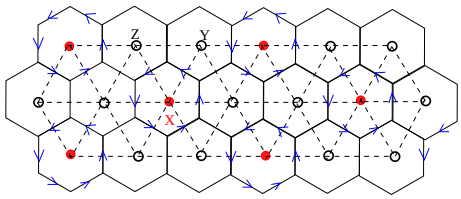

FIG. 2: The X-CDW state in the Ising limit $v > 0$ at $f = 1/3$. At $f = 2/3$, one can just reverse the current flow and perform a particle and hole transformation in $f = 1/3$, namely, exchange particles (red dots) and vacancies (black empty circles).

the I is the current flowing around the X lattice site in Fig.2. The $x \sim n_x - n_y > 0$ can be thought as a CDW order parameter and can be tuned by the distance away from the SF to the CDW transition in the Fig.3a. When one tunes the density $n_y = n_z = 0$ which stand for vacancies, then $n_x = 1$ which stands for one boson. This corresponds to the classical limit $t = 0$ in Eqn.1. With the quantum fluctuations $t > 0$, then $n_x < 1, n_y = n_z > 0$.

Sown in Fig.2 is a CDW state corresponds to bosons occupying one of the three sublattices X, Y, Z in Fig.1a, so it is 3 fold degenerate. Eqn.3 is an expansion around the uniform saddle point $< \nabla \times \vec{A} >= f = 1/3$ which holds in the SF and the VBS (to be discussed in section II-B). In the CDW state, the fact that there are currents flowing on the dual honeycome lattice indicates that the average densities are re-distributed. Because of sharp change of the saddle point from Eqn.3 in the SF side to Eqn.9 in the CDW side, we expect that the CDW to superfluid transition at exactly 1/3 filling in Fig.3a is first order.

Well inside the CDW phase, there is a large CDW gap Δ_{CDW}. When studying the physics at slightly away from $f = 1/3$ filling along the dashed line in Fig.3a, one has to choose a different saddle point where $< \nabla \times \vec{A}^x >= 1 - 2\alpha = n_x$, for the sublattice X and $< \nabla \times \vec{A}^{yz} >= \alpha = n_y = n_z$ for the two sublattices Y and Z should be used. The $\alpha \to \alpha_c < 1/3$ limit corresponds to approaching the CDW to the SF transition in Fig.3a from the CDW side, while the $\alpha \to 0^+$ limit corresponds to the classical limit $t/V_1 \to 0$. It is easy to see that there is only one vortex minimum ϕ_{yz} in such a staggered dual magnetic field with $\alpha < \alpha_c < 1/3$, so the effective action well inside the CDW state is:

$$\begin{aligned} \mathcal{L}_{CDW} &= |(\partial_\mu - iA^{yz}_\mu)\phi_{yz}|^2 + r|\phi_{yz}|^2 + u|\phi_{yz}|^4 + \cdots \\ &+ \frac{1}{4}(\epsilon_{\mu\nu\lambda}\partial_\nu A^{yz}_\lambda - 2\pi\delta f \delta_{\mu\tau})^2 \end{aligned} \quad (9)$$

where the vortices in the phase winding of ϕ_{yz} should be interpreted as the the boson number. Note that the gauge field $\vec{A}^x$ is always massive with a large CDW gap Δ_{CDW}, so was already integrated out in Eqn.9. In the direct picture discussed in the online supporting material in[33], the gauge field A^{yz}_μ stands for the uniform density fluctuation near $\vec{q} = 0$, while the A^x_μ stands for the staggered density fluctuation near $\vec{Q}_N = (2\pi/3, 0)$ which has a large CDW gap in Fig.22.

Eqn.9 has the structure identical to the conventional $q = 1$ component Ginzburg-Landau model for a " superconductor " in a "magnetic" field. It is easy to see that if $< \phi_{yz} >\neq 0$, the system is in the CDW state where both $\vec{A}^{yz}$ and $\vec{A}^x$ are massive (Fig.22a). If $< \phi_{yz} >= 0$, the system is in the CDW supersolid (CDW-SS) state where there is a gapless superfluid mode represented by the dual gauge field A^{yz}_μ in Fig.22b, it still has the gapped mode near $\vec{q} = \vec{Q}_N$, it also has the same lattice symmetry breaking patterns as the CDW state at 1/3 filling. Therefore we show that the CDW solid to the CDW-SS transition driven by the chemical potential is in the same universality class as that from a Mott insulator to a superfluid transition, therefore have exact exponents $z = 2, \nu = 1/2, \eta = 0$ with logarithmic corrections (Fig.3a). It is known the SF is stable against changing the chemical potential (or adding bosons) in Fig.3a. There must be a transition from the CDW-SS to the SF inside the window driven by the quantum fluctuation r in the Fig.3a. The universality class of this transition is likely to be first order.

In the direct lattice picture, we can simply renormalize away the sublattice X where the bosons sit and focus on the effective boson hopping on the two sublattices Y and Z which form a honeycomb lattice whose dual lattice is a triangular lattice (Fig.1a). Then the dual vortex action in the dual triangular lattice is given by Eqn.9. From this direct picture, we can see why a CDW SS can be realized much more easily in a triangular lattice than in a square lattice: *in a triangular lattice, the Y and Z sublattices still form a connected honeycomb lattices where bosons can move without going through the sublattice X* . While in a square lattice, in a checkboard CDW (see Fig.19a), bosons can not hop on sublattice A without going through sublattice B. So for a hard core boson, checkboard SS is unstable against phase separation because bosons can not hop on to the sublattice B. But in a soft core case, the checkboard SS could be stabilized be-

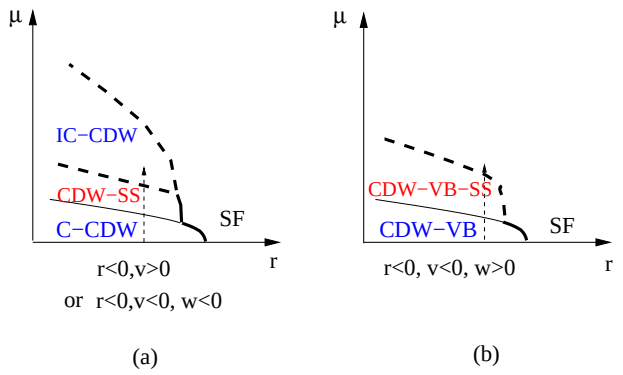

FIG. 3: Phase diagram of the EBHM in triangular lattice from the DVM in this paper. (a) The Ising limit $v > 0$. There is a CDW supersolid slightly above the 1/3 filling which has the same lattice symmetry breaking as the C-CDW in the Fig.2. The Easy-plane limit $v < 0, w < 0$. There is a stripe supersolid slightly above the 1/3 filling which has the same lattice symmetry breaking as the stripe in the Fig.4. (b) The Easy-plane limit $v < 0, w > 0$. There is a CDW-VB-SS slightly above the 1/3 filling which has the same lattice symmetry breaking as the CDW-VB in Fig.7. When the filling factor is increased further from the 1/3 filling, there is a first order transition from the CDW-SS (VB-SS) to In-commensurate CDW (or In-commensurate VBS). The IC-CDW or IC-VBS are stable only when there are sufficiently long range interactions. The thin (thick) line is the 1st (2nd) order transition. As shown in the text, the 1st order transition is a strong 1st order one in (a) and a weakly 1st order one in (b).

cause bosons can hop on the sublattice B too. A striped SS in a square lattice could be stabilized even in a hard core case, because boson can hop easily along one direction, so it is must easier for the bosons to overcome the barriers along the other direction to achieve an effective hopping.

B. Easy-plane limit $v < 0$.

If $v < 0$, the system is in the easy-plane limit, all the three vortex fields have equal magnitude $\phi_l = |\phi|e^{i\theta_l}$ and condense. Well inside the VBS side, the mean field solution holds. The relative phases can be determined by the sign of w. In the easy-plane limit, Eqn.3 is similar to the action in Tri-layer quantum Hall systems[29]. Introducing the center of mass, left and right moving modes as done in Ref.[29]: $\theta_c = \theta_0+\theta_1+\theta_2, \theta_l = \theta_0-\theta_2, \theta_r = \theta_0-2\theta_1+\theta_2$, Eqn.3 becomes:

$$\begin{aligned}\mathcal{L}_{VBS} &= (\frac{1}{3}\partial_\mu\theta_c - A_\mu)^2 + \frac{1}{4}(\epsilon_{\mu\nu\lambda}\partial_\nu A_\lambda - 2\pi\delta f\delta_{\mu\tau})^2 + \cdots \\ &+ \frac{1}{6}(\partial_\mu\theta_l)^2 + \frac{1}{18}(\partial_\mu\theta_r)^2 \\ &+ 2w\cos\frac{3\theta_l}{2}(\cos\frac{3\theta_l}{2} + \cos\frac{3\theta_r}{2}) \end{aligned} \quad (10)$$

In the bipartite lattices in a square and honeycomb

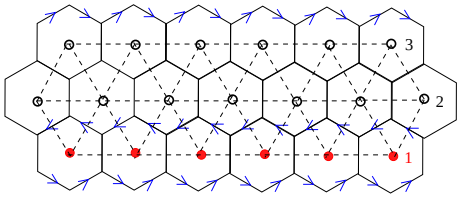

FIG. 4: The period 3 stripe phase in the easy plane limit $v < 0, w < 0$ at $f = 1/3$. At $f = 2/3$, one can just reverse the current flow and perform a particle and hole transformation in $f = 1/3$.

lattices[1,5], in the easy-plane limit, the system is always in a VBS state. As shown in the following, the easy-plane limit in a triangular lattice is much involved, in fact, there is always a CDW components, so it never corresponds to a pure VBS state.

(1) If $w < 0$, the mean field solution is $\theta_1 - \theta_0 = 2\pi m/3, \theta_2 - \theta_0 = 2\pi n/3$ where $m, n = 0, 1, 2$. Substituting $\theta_0 = \theta_1 = \theta_2 = 0$ into Eqns.2,6,7,8, one can evaluate the vortex densities, kinetic energy and the current in the dual honeycomb lattice. For simplicity, we only show the currents in the Fig.4 which are conserved. By counting the segments of currents along the bonds surrounding the three rows label, paying special attentions to their counter-clockwise or clock wise directions, we can calculate the densities at these points $n_1 = 1/3 + 4xI > 1/3, n_2 = n_3 = 1/3 - 2xI < 1/3$ where the I is the current flowing across the lattice. The $x \sim n_1 - n_2 > 0$ can be thought as a stripe order parameter and can be tuned by the distance away from the SF to the stripe transition in the Fig.3a. When one tunes the density $n_2 = n_3 = 0$ which stand for vacancies, then $n_1 = 1$ which stands for one boson. This corresponds to the classical limit $t = 0$ in Eqn.1. With the quantum fluctuations $t > 0$, then $n_1 < 1, n_2 = n_3 > 0$.

Well inside the stripe phase, it is legitimate to set $\theta_c = 3\theta_0 + \frac{2\pi}{3}(m+n), \theta_l = -\frac{2\pi}{3}n, \theta_r = \frac{2\pi}{3}(n-2m)$ in Eqn.10, the last term reaches its minimum $4w$. It is this w term which drives the formation of the stripe CDW in the Fig.4. There is a large stripe CDW gap $\Delta_{sCDW} \sim w$. When studying the physics at slightly away from $f = 1/3$ filling along the dashed line in Fig.3a, then Eqn. 10 reduces to Eqn.9. Then the discussions following the Eqn.9 also follow with the underlying CDW state as the stripe CDW state shown in Fig.4. The supersolid state is a stripe supersolid. The excitation spectra across the stripe to the stripe supersolid transition is also given by the Fig.22 with $\Delta_{sCDW} \sim w$. Alternatively, starting from the new saddle point for the dual gauge gauge fields corresponding to Fig.4: $< \nabla \times \vec{A}^1 >= 1 - 2\alpha = n_1$, for the row 1 and $< \nabla \times \vec{A}^{23} >= \alpha = n_2 = n_3$ for the row 2 and 3, one can construct the same effective action as Eqn.9 after making the replacement $x \to 1, yz \to 23$.

It is interesting to see that one is not able to get the stripe solid state from the DVM in bipartite lattices in[5] (see also appendix B and C), here one can get the stripe

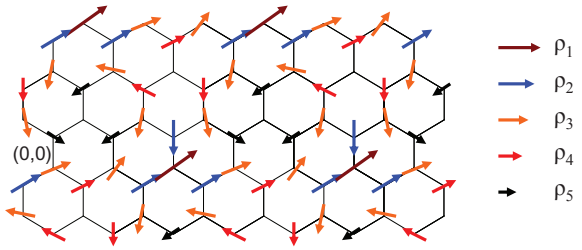

FIG. 5: The vortex field of the CDW-VB phase in a tr angular lattice in the easy plane limit $v < 0, w > 0$ a $f = 1/3$. Shown is $\theta_0 = 0, \theta_1 = 2\pi/9, \theta_2 = -2\pi/9$ case. The $(0,0)$ sets the origin. There are 5 different non-zero magnitudes shown with 5 different lengths: $\rho_1 = 3\sin(4\pi/9), \rho_2 = 4\sin(\pi/3)\cos(2\pi/9)\cos(\pi/9), \rho_3 = 2\sin(\pi/3)\cos(\pi/18), \rho_4 = 2\sin(\pi/3)\cos(2\pi/9), \rho_5 = \sin(\pi/3)$. Note particularly the lattice points where the vortex fields vanish ! The values of the vortex field are listed in the appendix A.

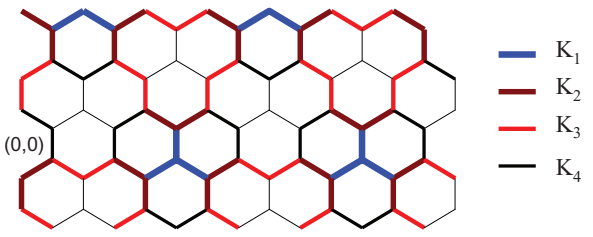

FIG. 6: The Kinetic energy of the CDW-VB phase in a triangular lattice in the easy plane limit $v < 0, w > 0$ at $f = 1/3$. Shown is $\theta_0 = 0, \theta_1 = 2\pi/9, \theta_2 = -2\pi/9$ case. The $(0,0)$ sets the origin. There are 4 different non-zero kinetic energies shown with 4 different colors: $K_1 = 12\sin(4\pi/9)\sin(\pi/3)\cos(2\pi/9)\cos(\pi/9), K_2 = 8\sin^2(\pi/3)\cos(2\pi/9)\cos(\pi/9)\cos^2(\pi/18), K_3 = 4\sin^2(\pi/3)\cos(2\pi/9)\cos^2(\pi/18), K_4 = 2\sin^2(\pi/3)\cos(5\pi/18)$. Note particularly the bonds where the kinetic energies vanish ! These bonds emanate from the lattice points where the vortex fields vanish, see the Fig.5

solid state from the DVM in a triangular lattice from a easy plane limit.

(2) If $w > 0$, one of the 18 equivalent solutions is $\theta_1 - \theta_0 = \theta_0 - \theta_2 = 2\pi/9$, then $\theta_1 - \theta_2 = 4\pi/9$. Substituting this solution into Eqns.2,6, we find the explicit values of the vortex fields at the two sublattices a and b of the dual honeycomb lattice graphically shown in Fig.5 and listed in the appendix D. Substituting the vortex field values in Eqn.D1 into Eqns. 7,8 one can evaluate the vortex densities in Fig.5, kinetic energy in Fig.6 and the current in Fig.7 By counting the number of currents along the bonds surrounding the red, green and black lattice points, paying special attentions to their counter-clockwise or clockwise directions, we can calculate the densities at these points $n_r = 1/3 + 2x[I_1 + (I_1 - I_2)] > 1/3, n_g = 1/3 + 2x[I_2 + (I_2 - I_1)] > 1/3, n_b = 1/3 - 2x[I_1 + I_2] < 1/3$ where $I_1 = \sin\frac{3\pi}{9} + \sin\frac{2\pi}{9} > I_2 = \sin\frac{\pi}{9} + \sin\frac{2\pi}{9}$. The x can be tuned by the distance away from the SF to the CDW+VB transition in Fig.3b. When one tunes the density $n_b = 0$, then $n_r = \frac{I_1}{I_1+I_2} > n_g = \frac{I_2}{I_1+I_2}$ with $n_r/n_g = I_1/I_2, n_r + n_g = 1$.

At $f = 2/3$ case, one only need to change $n_r \to \tilde{n}_r = 1 - n_r = 2/3 - 2x[I_1 + (I_1 - I_2)] < 2/3, n_g \to \tilde{n}_g = 1 - n_g = 2/3 - 2x[I_2 + (I_2 - I_1)] < 2/3, n_b \to \tilde{n}_b = 1 - n_b = 2/3 + 2x[I_1 + I_2] > 2/3$. When one tunes the density $n_b = 1$, the $n_r = \frac{I_2}{I_1+I_2} < n_g = \frac{I_1}{I_1+I_2}$ with $n_r + n_g = 1$. When one tunes the density $\tilde{n}_r = 0$, then $\tilde{n}_g = \frac{2(I_1-I_2)}{2I_1-I_2}, \tilde{n}_b = \frac{2I_1}{2I_1-I_2}$ with $\tilde{n}_g + \tilde{n}_b = 2$.

It is important to observe that as shown in the vortex field Fig.5, the vortex fields vanish both at the centers of the red loop and the green loop, therefore, both the kinetic energy and the current emanating from the centers vanish. This fact indicates that there are local SF (or VBS order) around the these two dual lattice points as shown by the red and green triangles in Fig.7. It is interesting to compare this with the known fact that interacting bosons in a kagome lattice at $f = 1/2$[3,25] are always in a SF state due to the localization of the vortices (a flat vortex band). The difference is that here there is only a local SF around the the centers of the red loop and the green loop, while there is a global SF across the whole lattice in the latter case. However, the vortex field is non-vanishing at the black point, so only the current vanishes, but the kinetic energy as shown in Fig.6 does not vanish, it shows there are local CDW around the dual lattice point as shown by black dots in the Fig.7. So this state has both VBS and CDW which can be called CDW-VB state, it is a mixed state unique to a frustrated lattice.

Well inside the CDW-VB phase, it is legitimate to set $\theta_c = 3\theta_0, \theta_l = -\frac{2\pi}{9}, \theta_r = -\frac{2\pi}{3}$ in Eqn.10, the last term reaches its minimum $-\frac{w}{2}$. It is this w term which drives the formation of the CDW-VB in the Fig.7. There is a large CDW-VB gap $\Delta_{CDW-VB} \sim |w|$. When studying the physics at slightly away from $f = 1/3$ filling along the dashed line in Fig.3b, then Eqn. 10 reduces to Eqn.9 Then the discussions following the Eqn.9 also follow with the underlying state as the CDW-SS state shown in Fig.7. The supersolid state is a CDW-VB supersolid. The excitation spectra across the CDW-VB to the CDW-CB SS transition is also given by the Fig.22 with $\Delta_{CDW-VB} \sim |w|$. Alternatively, starting from the new saddle point for the dual gauge gauge fields corresponding to Fig.7: $< \nabla \times \vec{A}^r >= n_r$ for the red site, $< \nabla \times \vec{A}^g >= n_g$ for the green site and $< \nabla \times \vec{A}^b >= n_b$ for the black site, one can construct a similar effective action as Eqn.9.

In Ref.[21], using the density operator formalism on a triangular lattice (See appendix D), the authors identified a bubble phase in Fig.25 which is a CDW state. This bubble CDW phase is completely different from the CDW-VB phase in Fig.7. It is important to identify the CDW-VB phase from the the density operator formalism. Some general problems associated with the density operator formalism are examined in appendix D.

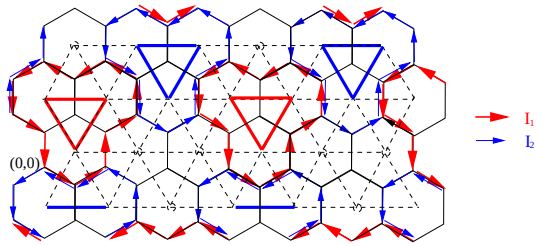

FIG. 7: The CDW-VB phase in a triangular lattice in the easy plane limit $v < 0, w > 0$ at $f = 1/3$. Shown is $\theta_0 = 0, \theta_1 = 2\pi/9, \theta_2 = -2\pi/9$ case. The $(0,0)$ sets the origin. The red current is $I_1 = \sin\frac{3\pi}{9} + \sin\frac{2\pi}{9}$, the blue current $I_2 = \sin\frac{\pi}{9} + \sin\frac{2\pi}{9}$. The currents are conserved at all the lattice points. At $f = 2/3$, one can just reverse the current flow and perform a particle and hole transformation in $f = 1/3$. For $\theta_0 = 0, \theta_1 = -2\pi/9, \theta_2 = 2\pi/9$, one only need to rotate the figure by 180°.

We conclude that the transitions from the X-CDW, stripe-CDW, CDW-VB solid to the corresponding supersolids driven by the chemical potential in the Fig.3 is also in the same universality class as that from a Mott insulator to a superfluid.

C. Valence bond state and absence of Valence bond supersolid in a triangular lattice

It is easy to draw the VBS state in a triangular lattice in the Fig.8 This is a plaquette state similar to the plaquette state in a square lattice shown in Fig.20b In contrast to the dimer VBS in a square lattice, there is no dimer VBS at a triangular lattice. So the uniform saddle point $< \nabla \times \vec{A} >= f = 1/3$ holds in both the SF and the VBS. As shown in the previous two sections, from the dual vortex theory, one is not able to get a pure VBS state at $f = 1/3$ shown in Fig.8 in either the Ising limit or easy-plane limit. Fig.7 contains the VB component, but also a CDW component. Because the excitation of this state necessarily involves a density excitation shown in Fig.11b, drawing the insights gained from the direct first order transition from a pure VB state to a SF in a Kagome lattice Fig.12 to be discussed in Sec.III-2, we conclude that there is no VB-SS in a triangular lattice, in sharp contrast to bipartite lattices discussed in[5] and in the appendix B and C, there can only be a direct first -order transition from the VB to the SF.

D. Implications on QMC simulations in triangular lattice

(1) Nearest Neighbor (NN) EBHM in a triangular lattice

The simplest EBHM in Eqn.1 is the hard core bosons hopping in a triangular lattice with only nearest neighbor

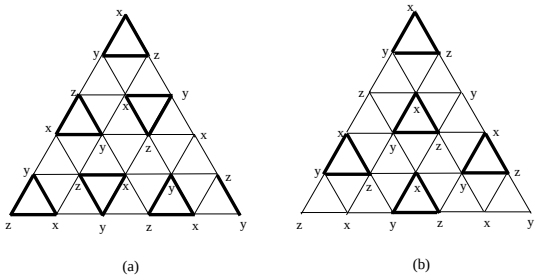

FIG. 8: Two kinds of valence bond solids (VBS) in a triangle lattice. (a) Uniform VBS state. (b) Staggered VBS state.

(nn) interaction $U = \infty, V_1 > 0$:

$$H_{nn} = -t \sum_{<ij>} (b_i^\dagger b_j + h.c.) + V_1 \sum_{<ij>} n_i n_j - \mu \sum_i n_i \quad (11)$$

This model was studied expensively by QMC in[17–20] where the hard core constraint $n_i = b_i^\dagger b_i \leq 1$ considerably reduces the size of Hilbert space in QMC simulations. The QMC results in[19,20] leads to Fig.9a. When comparing the Fig.3a In the Ising limit $r < 0, v > 0$ achieved in this paper with the Fig.9a by QMC, one can see that the solid state at 1/3 is just the X- solid state in Fig.2. the SS-i is just the CDW-SS. The IC-CDW state in Fig.3a can not be realized in Fig.9a, because it can only be stabilized by much longer-range interactions than V_1. The dual vortex effective action to describe the transition from the SF to the 6-fold solid is given by Eqn.3 in the Ising limit $r < 0, v > 0$, it was found to be very weak first order by QMC in[19,20]. The effective action to describe the transition from the 6-fold solid to the stripe supersolid slightly away from 1/3 is given by Eqn.9. However, the universality class of the 2nd phase transitions in Fig.2a was not studied in[19,20]. Comparing the QMC results with Fig.3a from the DVM, we can see the solid at 1/3 filling to the interstitial induced supersolid (SS-i) slightly above 1/3 filling is indeed second order transition in the same universality class as that from a Mott insulator to a superfluid. However, the SF to the SS-i is likely to be weakly first order. Note that sometimes it is difficult to distinguish a 2nd order transition from a weakly first order one from QMC. More refined QMC simulations are needed to address the nature of the SF to SS-i transition.

(2) Next Nearest Neighbor (NNN) EBHM in a triangular lattice: Stripe phase, Stripe-SS phase

The next simplest EBHM in Eqn.1 is the hard core bosons hopping in a triangular lattice with NN and next nearest neighbor (nnn) interactions $U = \infty, V_1 > 0, V_2 > 0$:

$$\begin{aligned} H_{nnn} &= -t \sum_{<ij>} (b_i^\dagger b_j + h.c.) + V_1 \sum_{<ij>} n_i n_j \\ &+ V_2 \sum_{<<ik>>} n_i n_{jk} - \mu \sum_i n_i \end{aligned} \quad (12)$$

It was studied by QMC in[23]. A period-3 striped soild state is found at $f = 1/3$ and a stripe-supersolid was found at slightly large than 1/3. The QMC results in[23] leads to Fig.9b. When comparing the Fig.3a in the easy plane limit $r < 0, v < 0, w < 0$ achieved in this paper with the Fig.9b by QMC, one can see that the stripe state at 1/3 is just the stripe state in Fig.4. The dual vortex effective action to describe the transition from the SF to the stripe solid is given by Eqn.3 in the easy plane limit $r < 0, v < 0, w < 0$, it was found to be strongly first order by QMC in[23]. The effective action to describe the transition from the stripe solid to the stripe supersolid slightly away from 1/3 is given by Eqn.9. However, the universality class of the 2nd phase transitions in Fig.9b was not studied either in[23].

(3) Searching for the CDW-VB phase in the NNN EBHM model in a triangular lattice

A meta-stable bubble solid phase in Fig.25 was also found in the QMC in[23]. This bubble solid phase has higher energy than the stripe solid phase. The very interesting CDW-SS phase in Fig.7 was not searched in the QMC in[23] in any parameter regimes. In order to identify this phase, in addition to the QMC calculations of the superfluid density and the density structure factor in[23], a bond structure factor[33] need also be studied to search for the VB ordering in the Fig.7.

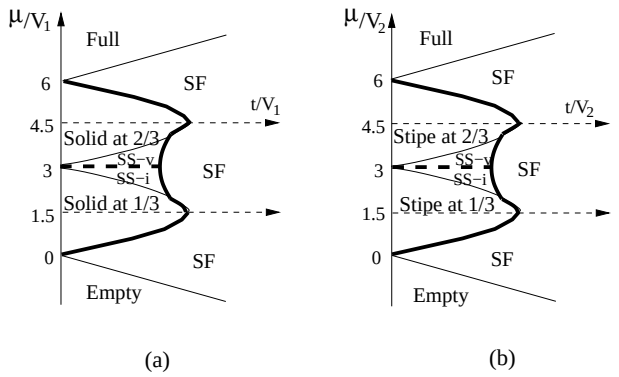

FIG. 9: (a) QMC results in[19,20] on triangular lattice with $U = \infty, V_1 > 0$. Slightly above (below) the 1/3(2/3) filling, there is a SS-i (SS-v) which has the same lattice symmetry breaking patterns as the solid at 1/3 (2/3) where the bosons occupying (un-occupying) one of the 3 sublattices X, Y, Z in Fig.1a. SS-i and SS-v are related by the P-H transformation. Exactly at half filling where $\mu/V_1 = 3$, SS-i and SS-v coexist at any possible ratio, there is a first order transition from SS-i to SS-v driven by the chemical potential μ across the thick dashed line. (b) Suggested phase diagram on triangular lattice with $U = \infty, V_1 = 0, V_2 > 0$ by the DVM in this paper. The Solid at 1/3 is the period-3 stripe phase studied numerically first in[23]. The SS-i slightly above 1/3 filling is the corresponding period-3 stripe supersolid phase studied by recent QMC in[23]. If the solid at 1/3 is the CDW-VB solid phase in Fig.7, then the corresponding possible CDW-VB SS phase maybe *unstable* against phase separation. The thin (thick) line is the 1st (2nd) order transition. As explained in the text, the first order transition is a strongly first order one. The universality class of the 2nd order phase transitions was not studied in[19,20,23].

III. SOLIDS AND SUPERSOLIDS IN KAGOME LATTICE NEAR 1/3(2/3)

The Kagome lattice (Fig.10a) has 3 sublattices a, b and c, its dual lattice is the dice lattice (Fig.10a). Due to too strong quantum fluctuations, as shown in[2] the spin wave expansion does not work anymore in Kagome lattice. Here I am trying to investigate the phases and quantum phase transitions when slightly away from the 1/3 filling from the DVM. Because of the P-H symmetry at $U = \infty$, the results are equally valid near 2/3 filling. As shown in[3] at $q = 2$, because the lowest dual vortex band in the dice lattice is completely flat, so the dual vortices are completely localized, so it has to be a superfluid, in sharp contrast to $q = 2$ on triangular lattice Fig.9. For $q = 3$, from Table 1 of[3], we can see there are two minima at $(0, 0)$ and $(-2\pi/3, 2\pi/3)$. Let's label the two eigenmodes at the two minima as $\phi_l, l = 0, 1$. The effective action invariant under all the MSG transformations upto sixth order terms was written down in[25]. Again, inside the superfluid phase, moving *slightly* away from the 1/3 filling $f = 1/3$ corresponds to adding a small *mean* dual magnetic field $\delta f = f - 1/3$ in the action derived in[25]. Upto sixth order, the action is $\mathcal{L}_{SF} = \mathcal{L}_0 + \mathcal{L}_1 + \mathcal{L}_2$:

$$\begin{aligned}
\mathcal{L}_0 &= \sum_l |(\partial_\mu - iA_\mu)\phi_l|^2 + r|\phi_l|^2 + \frac{1}{4}(\epsilon_{\mu\nu\lambda}\partial_\nu A_\lambda - 2\pi\delta f \delta_{\mu\tau})^2 \\
\mathcal{L}_1 &= u(|\phi_0|^2 + |\phi_1|^2)^2 - v(|\phi_0|^2 - |\phi_1|^2)^2 \\
\mathcal{L}_2 &= w[(\phi_0^* \phi_1)^3 + h.c.] \qquad (13)
\end{aligned}$$

where A_μ is a non-compact $U(1)$ gauge field.

In fact, the form of this action is *exactly the same* as that in honeycomb lattice at $q = 2$ first derived in[5]. However, the physical meanings of the two eigenmodes $\phi_l, l = 0, 1$ are completely different in the two lattices, this fact leads to completely different physics in the two lattices.

Ref.[25] studied the vortex environments in the dual dice lattices, but did not evaluate any gauge invariant physical quantities. The vortex enurements are gauge dependent, so may not be used to characterize the symmetry breaking patterns. Ref.[30] studied the bosons hopping on a Dice lattice at an integer filling. These bosons have only on-site interaction, but are subject to some artificial gauge fields which can be generated in cold atom experiments. They identified the vortex fields and the gauge invariant currents at $f = 1/3$. These artificial gauge fields are static. While the gauge field in all the dual vortex actions Eqn.13,16,14 on the dual Dice lattice are quantum fluctuating which are responsible for the very existences of the CDW-VB-SS.

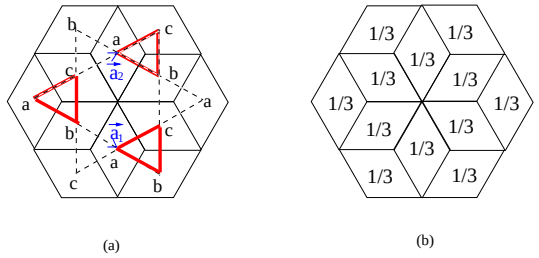

FIG. 10: (The VBS around the up triangle (triangular valence bond (TVB)) in a Kagome lattice in the Ising limit $v > 0$ at $f = 1/3$. The thick triangle means one at $f = 1/3$ (or two at $f = 2/3$) boson(s) is (are) moving around the up triangle. (b) The saddle point of the dual gauge field in a magnetic field unit cell in the dice lattice. The saddle point stays the same as that in the SF phase.

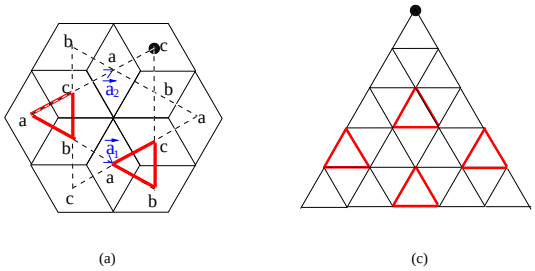

FIG. 11: A local density excitation above the TVB state in Fig.10. Its translational moving through the whole lattice leads to the excitation spectrum in the upper right Fig.12. Compare with the local excitation in a VBS in Fig.19.

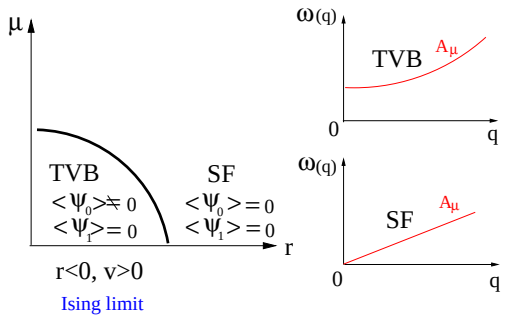

FIG. 12: The phase diagram driven by the chemical potential μ. There is a direct first order transition from the TVB to the superfluid. There is no supersolid intervening between the TVB and the SF in any case. Upper right is the gapless excitation due to the gauge field A_μ in the SF. Lower right is the gapped excitation due to the Higgs mechanism of the gauge field A_μ inside the TVB.

A. Ising limit, $v > 0$.

If $v > 0$, the system is in the Ising limit, only one of the 2 vortex fields condense. Let us take $\langle\phi_0\rangle \neq 0, \langle\phi_1\rangle = 0$. Using Eqns.7,8, one can evaluate both the vortex density, the kinetic energy and current in the dual dice lattice. This has been done in[30] in a very different context. There is no current flowing in the dual lattice which shows there is no CDW order. All the densities at the direct lattice are fixed at 1/3. It is important to point out that the vortex fields at the dual center of the red triangles in the Fig.10a vanish, so both currents and the kinetic energies emanating from these dual centers are vanishing, this fact indicates that there is a local VBS order around red triangles as shown in the Fig.10. This is just opposite to bipartite and triangular lattices discussed in[5] and the last section where the Ising limit corresponds to the CDW cases. This crucial difference is responsible for the absence of supersolid in the Ising limit as shown in the following. Because the saddle point structure stays the same across the SF to the triangle-VBS (TVB) transition at $f = 1/3$ as shown i the Fig12a, Eqn.13 still holds in the TVB side, so the transition is a *weak* first order one which breaks both the $U(1)$ and the Z_2 exchange symmetry between ϕ_0 and ϕ_1. In contrast, in the Ising limit of both the bipartite and triangular lattice, different saddle points for the dual gauge fields need to be chosen.

Slightly away from 1/3 filling, there must be a direct first order transition from the TVB to the superfluid as shown in Fig.12, there is no TVB supersolid intervening between the RVB and the SF, in sharp contrast to the cases in bipartite and triangular lattices.

Note that due to the lack of dimer VBS on the Kagome lattice at $f = 1/3$, any excitation above the TVB state in the Fig.10 will necessarily involve the breaking the the TVB into a density excitation shown in Fig.11. This gap is of density origin represented by the gauge field fluctuation in Eqn.13. This is in sharp contrast to the dimer VB or plaquette VB state in bipartite lattices such as square and honeycome lattice. In these bipartite lattices, there are VBS excitation gaps due to the operator $\lambda \cos 4\theta$ which only involves dimer flips instead of any density fluctuation shown in Fig.21. Here, such an operator is lacking in the Ising limit, so there is no such VBS gap.

B. Easy-plane limit $v < 0$.

If $v < 0$, the system is in the easy-plane limit, Eqn.3 is similar to the action in Bi-layer quantum Hall systems[32], the two vortex fields have equal magnitude $\phi_l = |\phi|e^{i\theta_l}$ and condense. The relative phases can be determined by the sign of w[5]. When moving from 1/3 to 1/2 where the bosons has to be in a SF state, Eqn.16 can be rewritten as:

$$\mathcal{L}_{VBS} = (\frac{1}{2}\partial_\mu\theta_+ - A_\mu)^2 + \frac{1}{4}(\epsilon_{\mu\nu\lambda}\partial_\nu A_\lambda - 2\pi\delta f\delta_{\mu\tau})^2 + \cdots + \frac{1}{2}(\partial_\mu\theta_-)^2 + 2w\cos 3\theta_- \quad (14)$$

where $\theta_\pm = \theta_0 \pm \theta_1$.

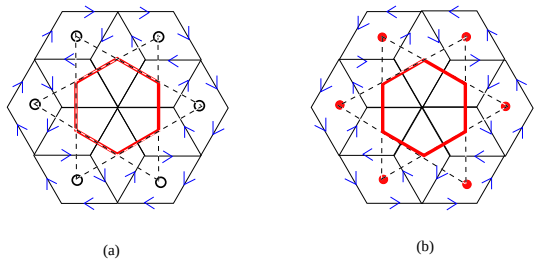

FIG. 13: The charge density wave + VBS state in a Kagome lattice in the easy-plane limit $v < 0, w > 0$ at (a) $f = 1/3$ (b) $f = 2/3$. The red solid circle is a boson, the empty red circle is an vacancy. (a) and (b) are related by time reversal symmetry and particle-hole symmetry.

In the following, we discuss both cases separately.

(1) $w > 0$. CDW+VBS order:

When $w > 0$, $\theta_- = \theta_0 - \theta_1 = (2n+1)\pi/3$, using Eqns.7,8, one can evaluate both the vortex density, the kinetic energy and current in the dual dice lattice. This has been done in[30] in a different context. The current was shown in the Fig.13. It is important to point out that the vortex at the dual center of the red hexagon vanishes which indicates the there is a local VB order around the dual center as shown by the red hexagon in the Fig.13. Again, it is interesting to compare this with the known fact that interacting bosons in a kagome lattice at $f = 1/2$[3,25] are always in a SF state due to the localization of the vortices (a flat vortex band). The difference is that here there is only a local SF around the the center of the red hexagon, while there is a global SF across the whole lattice in the latter case. By counting the segments of currents along the bonds surrounding the red and black lattice points, paying special attentions to their counter-clockwise or clock wise directions, we can calculate the densities at these points $n_b = 1/3 - 4xI < 1/3, n_r = 1/3 + 2xI > 1/3$ at the filling factor $f = 1/3$ where the I is the current flowing around the black lattice site in Fig.13. The $x \sim n_r - n_b > 0$ can be thought as a CDW-VB order parameter and can be tuned by the distance away from the SF to the CDW-VB transition in the Fig.3b. When one tunes the density $n_b = 0$ which stand for vacancies, then $n_r = 1/2$ which stands for 3 bosons are hopping around the the red hexagon to form a local VB order. Very similar calculations can be made for the filling factor $f = 2/3$ which is related to $f = 1/3$ by a particle-hole transformation shown in Fig.13b. 13b.

Well inside the CDW-VB phase, it is legitimate to set $\theta_- = \theta_0 - \theta_1 = (2n+1)\pi/3$ in Eqn.14, the last term reaches its minimum $-2w$. It is this w term which drives the formation of the CDW-VB phase in the Fig.10. There is a CDW-VB gap $\Delta_{CDW-VB} \sim w$. When studying the physics at slightly away from $f = 1/3$ filling along the dashed line in Fig.3a, then Eqn. 13 reduces to Eqn.14.

Alternatively, one can start from the new saddle point for the dual gauge gauge fields corresponding to Fig.14b which is $< \nabla \times \vec{A}_{CDW} >= n_b = 1 - \alpha, < \nabla \times \vec{A}_{VBS} >= n_r = (1+\alpha)/2$ as shown in Fig,3b. The lowest energy dual vortex band in such a saddle point is found to be:

$$\begin{aligned} E(k_1,k_2) &= -\sqrt{6 + 2A(k_1,k_2)}, \quad -\pi < k_1, k_2 < \pi \\ A(k_1,k_2) &= \cos k_1 - \cos(k_1 - \alpha\pi) + \cos k_2 - \cos(k_2 + \alpha\pi) \\ &+ \cos(k_1 - k_2) - \cos(k_1 - k_2 - 2\alpha\pi) \end{aligned} \quad (15)$$

It is easy to see that there is a symmetry $E(k_1,k_2) = E(k_2 + \pi(1+\alpha), k_1 + \pi(1-\alpha))$. For $0 < \alpha < 0.404$, there are two minima at $k_1 = \alpha\pi/2 - arcsin(\frac{\sin(\alpha\pi/2)}{2\cos(\alpha\pi)}), k_2 = -k_1$ and $k_1 = \alpha\pi/2 + arcsin(\frac{\sin(\alpha\pi/2)}{2\cos(\alpha\pi)}) + \pi, k_2 = -k_1$. The two minima are related by the symmetry.

When $\alpha = 1/3 < 0.404$, it reduces to $q = 3$ case where there are two minima at $(0,0), (-\frac{2\pi}{3}, \frac{2\pi}{3})$ which is the two minima at the superfluid side. The $\alpha \to 1/3^-$ case corresponds to approaching to the transition from the CDW+VB to the SF in Fig.3b from the left hand side. For $\alpha = 0$ which corresponds to $t/V_1 \to 0$ limit in Fig.17a, $A(k_1,k_2) = 2\cos(k_1 - k_2)$, then the minima is along the line $k_1 = k_2$, the band is flat along this direction. At $q = 2$, the band is completely flat as shown in[3]. In fact, when $\alpha = 0$, all the 6 parallelograms around the center in the Fig.14b have $q = 2$, the other 6 have $q = 1$, so it is not a surprising that the band is flat along one direction. Of course, for $\alpha = 1$, it reduces to the zero magnetic case $q = 1$ where there is only one minimum at $(0,0)$.

Now for $0 < \alpha < 1/3^-$, because the two minima are smoothly connected to those in the SF side, let's still label the two minima by $\phi_l, l = 0, 1$. Then the MSG inside the SF state $T_1, T_2, R_{\pi/3}, I_1$ is reduced to $T_{\vec{a}_1+\vec{a}_2}, R_{\pi/3}, I_{\vec{a}_1+\vec{a}_2}$ inside the CDW+VBS state in Fig.14. Note that only the translational symmetries are reduced, but the rotational symmetry remains the same as inside the SF state. The effective action slightly away from 1/3 invariant under the MSG transformations inside the CDW+VBS state upto sixth order terms is $\mathcal{L}_{CDW+VBS} = \mathcal{L}_0 + \mathcal{L}_1 + \mathcal{L}_2$:

$$\begin{aligned} \mathcal{L}_0 &= \sum_l |(\partial_\mu - iA^{VBS}_\mu)\phi_l|^2 + \tilde{r}|\phi_l|^2 + \frac{1}{4}(\epsilon_{\mu\nu\lambda}\partial_\nu A^{VBS}_\lambda - 2\pi\delta f \delta_{\mu\tau})^2 \\ \mathcal{L}_1 &= \tilde{u}(|\phi_0|^2 + |\phi_1|^2)^2 - \tilde{v}(|\phi_0|^2 - |\phi_1|^2)^2 \\ \mathcal{L}_2 &= \tilde{w}[(\phi_0^* \phi_1)^3 + h.c.] \end{aligned} \quad (16)$$

where A^{VBS}_μ is a non-compact $U(1)$ gauge field.

Note that Eqn.13 in the SF side and Eqn.16 in the CDW+VB side take the same form despite the reduced translational symmetry in the CDW+VB state. Note that A^{CDW}_μ is always massive, so was already integrated out in Eqn.16. Because the system is already in the CDW+VBS, so we expect $\tilde{r} < 0$ and $\tilde{v} < 0$. Then we can set $\phi_l = |\phi| e^{i\theta_l}$. The relative phases can be determined by the sign of $\tilde{w}$ which has the same sign as $w > 0$. Because of the very weak relevance of w term in Eqns.13 and 16, so we expect the SF to the CDW+VB transition driven by r is very weakly first order. This is in sharp contrast to the strong 1st order CDW to the SF transition in a triangular lattice in Fig.3a and Fig.9a. This

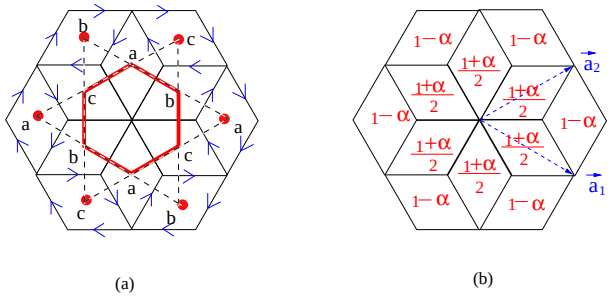

(a) (b)

FIG. 14: (a) The CDW+VBS in a Kagome lattice at $f = 2/3$ identified in[26]. The dot means one (or $1-\alpha$) boson occupying the site. The ◯ inside the hexagon means 3 (or $3(1+\alpha)$) bosons hopping around the hexagon. It has 3 sublattices labeled as a, b, c. (b) The saddle point of the dual gauge field in a magnetic field unit cell in the dice lattice. $\alpha = 0$ corresponds to (a). The $\vec{a}_1$ and $\vec{a}_2$ are the two basis vectors in the dual dice lattice

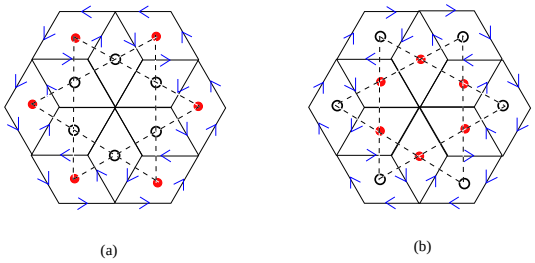

(a) (b)

FIG. 15: The 6-fold CDW state in a Kagome lattice in the easy-plane limit $v < 0, w < 0$ (a) $f = 1/3$ (b) $f = 2/3$. The red solid circle is a boson, the empty red circle is an vacancy. (a) and (b) are related by time reversal symmetry and particle-hole symmetry.

is exactly what were observed in the QMC in triangular lattice[19,20] and in kagome lattice[26].

When moving from 1/3 to 1/2 where the bosons have to be in a SF state, Eqn.16 also reduces to Eqn.14. The phase diagram may be similar to Fig.3b in the triangular lattice. The SS slightly away from 1/3 filling has the same CDW and VB order as the solid at 1/3, so let's call this kind of novel SS as CDW-VB-SS. Then the transition from the CDW+VB to the CDW-VB-SS transition driven by the chemical potential can be similarly discussed as the VBS to the VB-SS in bipartite lattices[5], so it is is the same universality class as that from the Mott insulator to the SF. The CDW-VB-SS to the SF transition is 1st order. Although the CDW-VB-SS is not stable in the hard core case, it is stable in the soft core case. Of course, there is no P-H symmetry anymore in the soft core case. This study may inspire more accurate QMC to search for this novel CDV-VB-SS state, especially in the soft-core case. The excitation spectra across the CDW-VB to the CDW-VB supersolid transition is also given by the Fig.22 with $\Delta_{CDW} \sim w$ or equivalently by Fig.25 with $\Delta_{VBS} \sim w$.

However, Eqn.16 may break down as $\alpha \to 0$ which corresponds to $t/V_1 \to 0$ limit, because the two minima become very shallow. At $\alpha = 0$, the band is flat along $k_1 = k_2$, so we expect the regime of the CDW + VB-SS shrinks to zero as $t/V_1 \to 0$ as shown in Fig.17a.

(2) $w < 0$ case: 6-fold CDW order:

When $w < 0$, $\theta_- = \theta_0 - \theta_1 = 2n\pi/3$, using Eqns.7,8, one can evaluate both the vortex density, the kinetic energy and current in the dual dice lattice. This has been done in[30] in a very different context. The current was shown in the Fig.15. It is important to point out that the vortex at the dual center of the black spots is non-vanishing, so only the current is zero due to the cancelation of the current flowing on the neighboring black points, but the kinetic energy is positive. This fact indicates the there is a local CDW order around the dual center as shown in the Fig. 15. By counting the segments of currents along the bonds surrounding the red and black lattice points, paying special attentions to their counter-clockwise or clock wise directions, we can calculate the densities at these points $n_r = 1/3 + 4xI > 1/3, n_b = 1/3 - 2xI < 1/3$ where the I is the current flowing around the red lattice site in Fig.15. The $x \sim n_r - n_b > 0$ can be thought as a CDW order parameter and can be tuned by the distance away from the SF to the CDW transition in the Fig.3a. When one tunes the density $n_b = 0$ which stand for vacancies, then $n_r = 1$ which stands for one boson. This corresponds to the classical limit $t = 0$ in Eqn.1. With the quantum fluctuations $t > 0$, then $n_r < 1, n_b > 0$. In fact, the 6-fold CDW state Fig.15 has the same symmetry as the CDW-VB state in Fig.13. The only difference is the local CDW order versus a local VBS order.

Well inside the 6-fold CDW phase, it is legitimate to set $\theta_- = \theta_0 - \theta_1 = 2n\pi/3$ in Eqn.14, the last term reaches its minimum $2w$. It is this w term which drives the formation of the 6-fold CDW in the Fig.15. There is a 6-fold CDW gap $\Delta_{CDW} \sim w$. When studying the physics at slightly away from $f = 1/3$ filling along the dashed line in Fig.3a, then Eqn. 13 with $w < 0$ reduces to Eqn.14 with $w < 0$. The discussions following the Eqn.14 also hold with the underlying CDW state as the 6 fold CDW state shown in Fig.15. The supersolid state is a 6 fold CDW supersolid. The excitation spectra across the 6-fold CDW to the 6-fold CDW supersolid transition is also given by the Fig.22 with $\Delta_{CDW} \sim w$. Alternatively, starting from the new saddle point for the dual gauge gauge fields which is identical to that of the CDW-VB phase shown in Fig.14b, one can also derive Eqn.14 and use its following discussions.

C. Stripe-CDW order:

As shown in the previous two sections, one is not able to get the stripe state at $f = 1/3$ in Fig.16 from the dual vortex theory in either the Ising limit or easy-plane limit. But it is very easy to get this state from the NNN

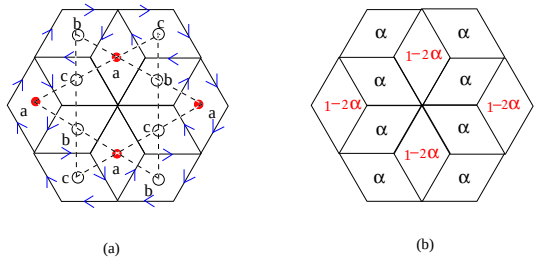

(a) (b)

FIG. 16: (a) The stripe CDW in a Kagome lattice at $f = 1/3$. The dot means one (or $\alpha > 1/3$) boson occupying a site in lattice a. (b) The saddle point of the dual gauge field in a magnetic field unit cell in the dice lattice. Compare the saddle point with Fig.14b

EBHM Eqn.12 in a Kagome lattice. If we add very strong nnn interaction V_2, the bosons will go to the nnnn which belong to a again (Fig.16), then the bosons will simply take one of the 3 sublattices such as a to form a CDW alone (Fig.16). Slightly away from 1/3, there is a stripe SS as shown in Fig.17b.

In the direct lattice Fig.16a, even if taking away the sublattice a, the bosons can still move easily along the chain *bcbc...*, so they need only overcome the barrier along the chain *baba...* to achieve an effective hopping along *baba....* So the superfluid stiffness along the *bc* chain is larger than that along the *ba* chain. In the stripe CDW state in Fig.16a, a different saddle point where $< \nabla \times \vec{A}^a >= 1-2\alpha$ for the sublattice a and $< \nabla \times \vec{A}^{bc} >= \alpha$ for the two sublattices b and c should be used. The $\alpha \to \alpha_c < 1/3$ limit corresponds to approaching the stripe CDW to the SF transition in Fig.17b from the stripe CDW side, while the $\alpha \to 0^+$ limit corresponds to $t/V_1 \to 0$ limit in Fig.17b. It is easy to see that there is only one vortex minimum ϕ_{bc} in such a staggered dual magnetic field with $\alpha < \alpha_c < 1/3$, so the effective action inside the stripe CDW state should be the same as Eqn. 9 with $yz \to bc$. Because of sharp change of the saddle point from Eqn.13 in the SF side to Eqn.4 in the stripe CDW side, so the transition from the SF to the stripe CDW along the horizontal axis in Fig.17b is likely to be a strong first order. Then the stripe-CDW to the stripe-SS transition driven by the chemical potential along the vertical axis is s second order transition

D. Implications on QMC simulations in Kagome lattice

(1) Nearest Neighbor (NN) EBHM in a Kagome lattice

Eqn.1 in Kagome lattice with $U = \infty, V_1 > 0$, namely, Eqn.11 in a Kagome lattice, was studied by two recent QMC simulations[26,27]. It was found that the solid state at exactly 1/3 filling has both CDW and VB order. The VB order corresponds to boson hopping around a hexagon (shown in Fig.13b). This is a unique feature of the Kagome lattices. This feature can be intuitively understood without any calculation: with very large V_1 interaction at 1/3 filling, if a boson taking sublattice c, then all its 4 nn which belong to sublattices a and b are excluded, so bosons will go to the 4 nnn which still belong to a and b instead of c (Fig.16a). This is in sharp contrast to triangular lattice at 1/3 filling in Fig.1a. So bosons may move around the hexagon to form some VB order in addition to the CDW order. This state is identical to the CDW-VB state in Fig.13a. Although the QMC in Ref.[27] found the the SF to the CDW+VB transition is a 2nd order transition through a noval deconfined quantum critical point[22], the QMC in Ref.[26] found a weakly 1st order transition from a double-peaked histogram of the boson kinetic energy. The dual vortex effective action to describe the transition from the SF to the CDW+VB is given by Eqn.13 in the easy plane limit $r < 0, v < 0, w > 0$. As explained below Eqn.16, it should be a weakly 1st order transition from the CDW-VB solid to the SF which is consistent with the conclusion in[26].

The effective action to describe the transition from the stripe solid to the stripe supersolid slightly away from 1/3 is given by Eqn.16. Drawing the insights gained from the square lattice[5], we conclude that the CDW-VB-SS is unstable against the phase separation in the hard core limit studied in[26,27]. But it will be stable in the soft core case.

(2) Next Nearest Neighbor (NN) EBHM in a Kagome lattice

It may be interesting to do QMC with $U = \infty, V_1 > 0, V_2 > 0$ to test Fig.17b. The hamiltonian is the same as Eqn.12, but in a Kagome lattice. As elucidated in the last paragraph, when both V_1 and V_2 are large, a CDW state where bosons simply take one of the 3 sublattices can be stabilized. Because the nn and the nnn neighbors are similar as can be seen from Fig.6a, the vertical axis in Fig.17b need to be replaced by $\mu/(V_1+V_2)$, the horizontal axis stay as t/V_1 at fixed large V_2 (Fig.17b). While the conclusion achieved in[3] that the system has to be a superfluid state at 1/2 remains robust. So we conclude that when moving from 1/3 to 1/2, the system goes CDW to stripe-SS to the SF transition. The first is the second order, the second is a first order transition (Fig.17b). Again, longer-range interactions favor the description in terms of the dual vortices and the stability of SS, so the Stripe-SS will surely be stable even in the hard core case (Fig.17b).

(3) Searching for the TVB state: possible ring exchange interactions

So far, the TVB state has not been identified in any QMC simulations. The ring exchange interaction $-K_k \sum_{ijkl} (b_i^\dagger b_j b_k^\dagger b_l + h.c.)$ where i, j, k, l label the 4 corners of a bow tie in the Kagome lattice is needed maybe stabilize this TVB phase.

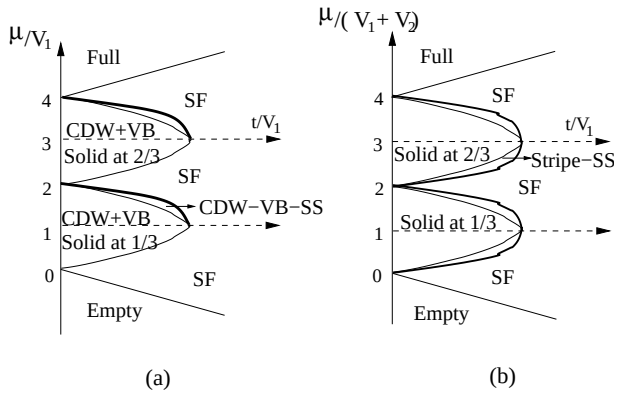

FIG. 17: (a) Suggested zero temperature phase diagram in Kagome lattice $U = \infty, V_1 > 0$. In the soft core case $U < \infty$, there maybe a narrow window of CDW-VB-SS sandwiched between the CDW-VB solid and the SF. Of course, there is no P-H symmetry anymore in the soft core case. In the hard core case studied in[26,27], the CDW-VB-SS is unstable, there is a direct weakly first order transition from the CDW-VB solid to the SF. Thin (thick) line is 2nd (first) order transition. It was shown in[3] that at half filling $f = 1/2$ where $\mu/V_1 = 2$, it can only be a SF state, in sharp contrast to $q = 2$ on triangular lattice Fig.9. (b) Very similar phase diagram also works for $U = \infty, V_1 > 0, V_2 > 0$. In this case, V_1 in (a) need to be replaced by $V_1 + V_2$, the solid at 1/3(2/3) is simply a CDW where the bosons occupying (un-occupying) one of the 3 sublattices a, b, c in Fig.16a. The SS is simply a stripe SS where the superfluid stiffness $\rho_{s1} \gg \rho_{s2}$. The Stripe-SS will surely be stable even in the hard core case. As shown in the text, the first order transition in (a) is a weakly first order one, but strongly first order one in (b)

IV. CONCLUSIONS

In summary, we used the DVM developed in[1,4,5] to study quantum phases, especially various kinds of insulating phases and phase transitions in the two most common frustrated lattices such as triangular and kagome lattices at and slightly away 1/3 and 2/3 fillings. At the commensurate fillings 1/3(2/3), we developed a systematic way to identify the symmetry breaking insulating states uniquely and completely by using gauge invariant vortex density, kinetic energy and current on the dual lattices. We reproduced several known phases found by the previous methods, also identified several new phases. We contrast different symmetry breaking patterns of the insulating phases in both Ising and Easy plane limits in the two lattices. By analyzing carefully the saddle point structures of the dual gauge fields in the translational symmetry breaking side and pushing the effective action slightly away from the commensurate fillings, We classified all the possible types of supersolids and analyze their stability conditions. By using these effective actions, we studied different kinds of solids, different kinds of supersolids and the universality class of quantum phase transitions from the solids to the supersolids. We also compared our results achieved by the DVM with some available QMC results and make implications on possible future QMC simulations. The results achieved in this paper should have direct impacts on ultra-cold atoms loaded on optical lattices. Although supersolids on lattices are different than that in continuous systems such as ^4He[38] or exciton supersolid in electron-hole bilayer system in[39], they may share some common properties and shed considerable lights on each other.

The DVM is a magnetic space group (MSG)[1] symmetry-based approach which, in principle, can be used to classify all the possible phases and phase transitions. But the question if a particular phase will be stable or not as a ground state depends on the specific values of all the possible parameters in the EBHM in Eqn.1, so it can only be addressed by a microscopic approach such as Quantum Monte-Carlo (QMC) simulations. The DVM can guide the QMC to search for particular phases and phase transitions in a specific model. Finite size scalings in QMC in a microscopic model can be used to confirm the phases and the universality classes of phase transitions discovered by the DVM. The two methods are complementary to each other and both are needed to completely understand phases and phase transitions in Eqn.1.

In the square lattices, so far, there are several established examples of nice comparisons between the phenomenological DVM and the QMC simulations on a microscopic model: (1) The transition from the SF to the X-CDW (Fig.19a) in the Ising limit $v > 0$ in a square lattice was studied by the DVM[1] and the QMC on the EBHM Eqn.11 with NN interaction in a square lattice at $f = 1/2$ with both hard[34] and soft core[35] bosons. (2) The transition from the SF to the X-CDW (Fig.19b) in the Ising limit $v > 0$ in a honeycomb lattice was studied by the DVM[5] and the QMC on the EBHM Eqn.11 with NN interaction in a honeycomb lattice at $f = 1/2$ with both hard and soft core bosons[24]. Unfortunately, there are still many cases the DVM and QMC can not be compared with each other. For example, the DVM is not able to get the stripe-solid phase studied extensively by QMC[34] on the EBHM of hard core bosons with NNN interaction Eqn.12 at $f = 1/2$. Interestingly, the stripe solid phase Fig.4 in a triangular lattice has been achieved by the DVM in the easy plane limit $v < 0, w < 0$. However, the stripe solid phase Fig.16a can not be achieved from the the DVM either. It remains an open problem how to achieve the strip solid phases in a square and kagome lattices by the DVM. On the other hand, so far, it has not been possible to study all the VBS phases by QMC in some microscopic models in the easy-plane limit of the DVM listed in the Fig.20 and Fig.23. The above two connections are established only in the Ising limit. This maybe due to the fact that a ring exchange interaction may be needed to stabilize all these VBS phases. It is still not known what are the specific forms of these ring exchange interactions.

In the frustrated lattices, so far, there are also sev-

eral established examples of nice comparisons between the phenomenological DVM and the QMC simulations on a microscopic model. For example, The DVM[3,25] predicted that the Kagome lattice at 1/2 must be a superfluid due to the complete flat band of the dual vortices. No insulating phases can be found at 1/2. This has been confirmed by QMC[26]. In the following, we list the connections directly relevant to this paper: (1) The transition from the SF to the X-CDW (Fig.2) in a triangular lattice at $f = 1/3$ was studied by the DVM in[21] in the Ising limit $v > 0$ of the effective action Eqn.3 and also by the QMC[17–20] on the EBHM of hard core bosons with NN interaction Eqn.11. (2) The transition from the SF to the Stripe-CDW (Fig.4) in a triangular lattice at $f = 1/3$ was studied by the DVM in[21] in the easy plane limit $v < 0, w < 0$ of the effective action Eqn.3 and also by the QMC[23]on the EBHM of hard core bosons with NNN interaction Eqn.12 at $f = 1/3$ in a triangular lattice. (3) The transition from the SF to the CDW-VB phase in a Kagome lattice at $f = 2/3$ was studied by the DVM in[25] and this paper in the easy plane limit $v < 0, w > 0$ of the effective action Eqn.13 and the QMC on the EBHM of hard core bosons with NN interaction Eqn.11 at $f = 2/3$ in a Kagome lattice.

In this paper, by using the method developed in this paper, we confirmed the first two and established the third explicitly for the first time. The first connection is on Ising limit. It was known that the transition is likely to be first order in the Ising limit. The last two are the only two known examples so far realized in the easy plane limit where there is some chance to realize the DCQCP[22] from the DVM. The last one is the only known example involving some VB order where there is a better chance to realize the DCQCP from the DVM. The advantage of the frustrated lattices over the bipartite lattices are that local VBS order can be realized in the former even without any ring exchange interaction. Unfortunately, both cases came up as negative. The first is a strong first order transition. From the DVM in Sect.II-B-1, it is related to a sharp change of the saddle point structure of the dual gauge field from the SF to the stripe CDW phase. The second is a very weak first order transition which needs some high power QMC technique such as double-peaked histogram to distinguish the very weak first order from a possible second order transition. From the DVM in Sect.III-B-1, we showed that the form of effective action in the CDW-VB side is identical to that in the SF side despite the reduced translation symmetry in the CDW-VB side. This gives an intuitive explanation why the transition is a very weak first order due to the very weak relevance of the $w \cos 3\theta$ term.

We also inspired furthermore comparisons between the two approaches. For example, the CDW+VB order in Fig.7 was not even searched in the QMC in[23] in any parameter regimes. We suggest to measure the bond-bond correlation to identify this interesting state by the QMC in[23]. We also suggest the QMC simulations of the EBHM Eqn.12 with NNN interaction in a Kagome lattice at 1/3 to search for a stripe solid phase and a stable stripe supersolid phase slightly away from 1/3. It is still not known how to realize the TVB phase in the triangular lattice Fig.8 and in a Kagome lattice Fig.10 by a microscopic model. However, it was shown that the excitation spectra above the TVB phase is necessarily of a density wave origin, so there is no TVB supersolid phase in both triangular and Kagome lattice. We expect more examples along these comparisons are needed to have a complete picture of phases and phase transitions from the two complementary approaches.

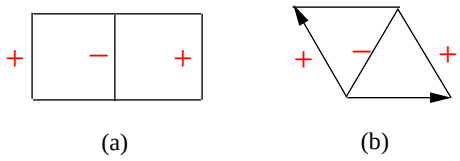

FIG. 18: The bond phase factors in bipartite lattices at half-filling. (a) dual square lattice (b) dual triangular lattice.

Acknowledgements

We thank Fuchun Zhang and Zidan Wang for the hospitality during our visit at Hong Kong university which initiated the collaboration. We also than Jianqiang You for his hospitality during J. Ye's visit at Fudan university. J.Ye thank G.G. Batrouni and S. V. Isakov for very helpful discussions, Longhua Jiang for technical assistances in finding the saddle point structures in the Kagome lattice, M. Boninsegni for helpful discussions on the QMC results in[20], Han Pu for his hospitalities during his visit at Rice university. Y. Chen thanks Yaowu Guo for technical assistances. Y. Chen's research was supported by the National Natural Science Foundation of China (Grant No. 10874032), the State Key Programs of China (Grant no. 2009CB929204) and Shanghai Municipal Government.

Appendix A: Magnetic space group in a square lattice

In this appendix, we apply the same method in the Section II to study the symmetry breaking insulating states in a square lattice. We only focus at the $q = 2$ case. We reproduced the results achieved in[1] using the operator formalism. Obviously, our method leads to much more intuitive and physical identification of these states. Fig.20a,b and Fig.19a have also been previously identified in[31] in the context of Z_2 gauge theory of high temperature superconductors. However, we disagree with their arguments leading to Fig.20b of the plaquette state. We believe this disagreement involves different physical interpretation of a local VBS state which are very important for the identifications of all the important phases in frustrated lattices discussed in the main text. Furthermore, we also explicitly give elementary excitation spectra in the dimer and plaquette VBS state.

The Harper's equation at $q = 2$ in a square lattice[3]

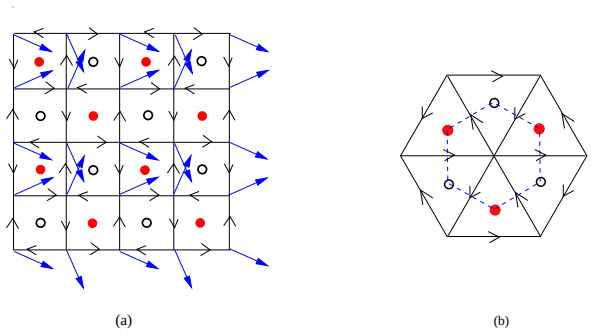

FIG. 19: (a) The X-CDW in the Ising limit in a square lattice. The vortex fields $\psi(0,0) = 1-(\sqrt{2}-1)i, \psi(0,1) = 1+(\sqrt{2}-1)i, \psi(1,0) = (\sqrt{2}-1)-i, \psi(1,1) = (\sqrt{2}-1)+i$. The vortex current flowing counter clockwise is $I = \sqrt{2}-1$. All the bonds have the same strength $K = \sqrt{2}-1$. There are no frustrated bonds. The vortex current flowing counter clockwise is $I = \sqrt{3}/2$. All the bonds have the same strength $K = 1/2$. There are no frustrated bonds. Following the current counting methods in the main text, one can see the density at the red site is $n_r = 1/2 + 4xI$, that at the black spot is $n_b = 1/2 - 4xI$. The $x \sim n_r - n_b$ tunes the distance away from the SF to the CDW transition. When $n_b = 0$, then $n_r = 1$ which corresponds to the classical limit $t/V_1 = 0$. (b) Ising limit in a honeycomb lattice.

leads to $c_m(l=0) = c_m = (1, \sqrt{2}-1)$. $\omega = e^{i2\pi f} = -1$. Denoting the dual square lattice site by $\vec{x} = (a_1, a_2)$. The vortex operator is:

$$\begin{aligned}\psi(\vec{x}) &= \sum_{m=0}^{1} c_m e^{i\pi m a_1}[\xi_0 + \xi_1 \omega^{-m} e^{i\pi a_2}] \\ &= \sum_{m=0}^{1} c_m (-1)^{m a_1}[\xi_0 + \xi_1 (-1)^m (-1)^{a_2}] \quad \text{(A1)}\end{aligned}$$

In the permutative representation:

$$\begin{aligned}\xi_0 &= (\phi_0 + \phi_1)/\sqrt{2} \\ \xi_1 &= -i(\phi_0 - \phi_1)/\sqrt{2} \quad \text{(A2)}\end{aligned}$$

In the Ising case $v > 0$: $\phi_0 = 1, \phi_1 = 0$, the vortex fields, kinetic energies and currents are shown in Fig.19a

In the easy plane limit[1] $v < 0$, there are also two cases depending on the signs of the quartic term $\lambda \cos 4\theta$:

(A) If $\lambda > 0$, then $\phi_0 = \phi_1 e^{in\pi/2}, n = 0,1,2,3$. The vortex fields, kinetic energies of the $n = 0$ case with $\phi_0 = \phi_1 = 1$ is shown in Fig.20a. It is a dimer state.

(B) If $\lambda < 0$, then $\phi_0 = \phi_1 e^{i(n+1/2)\pi/2}, n = 0,1,2,3$. The vortex fields, kinetic energies of the $n = 0$ case with $\phi_1 = 1$ is shown in Fig.20b which is plaquette state.

The corresponding local low energy excitations in the dimer and plaquette states are shown in the Fig.21. Because the density remains uniform, so there is no associated density wave excitation. The translational moving

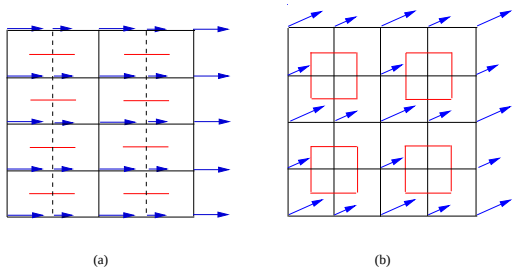

FIG. 20: The ground states in the easy-plane limit $v < 0$ in a square lattice (a) Dimer state at $\lambda > 0$. The long arrow is $\sqrt{2}$, the short arrow is $\sqrt{2}(\sqrt{2}-1)$. The dashed line is the frustrated vortex bond with strength $K_{fv} = -2(\sqrt{2}-1)^2$. The un-frustrated vertical vertex bond is $K_v = 2$. The horizontal bond is $K_h = 2(\sqrt{2}-1)$. The red bond which is perpendicular to the frustrated vortex bond is the boson valence bond in the direct lattice. The bosons are hopping back and forth along the red bond. (b) Plaquette state at $\lambda < 0$. The vortex fields $\psi(0,0) = 2[1+(\sqrt{2}-1)i], \psi(0,1) = \sqrt{2}[1+(\sqrt{2}-1)i], \psi(1,0) = \sqrt{2}[1+(\sqrt{2}-1)i] = \psi(0,1), \psi(1,1) = 0$. The arrows indicate both the magnitude and the phase of the vortex fields. Because the vortex field vanishes at $(1,1)$, so there is a local superfluid (or local VB order) around this dual lattice point as indicated by the red plaquette. The kinetic energies emanating from the zero vortex field points are also zero. All the other bonds have strength $K = 8(\sqrt{2}-1)$. The bosons are hopping around the red plaquette. There are no frustrated bonds. There are no vortex currents in both (a) and (b) indicating no CDW order, so the boson densities are fixed at $f = 1/2$.

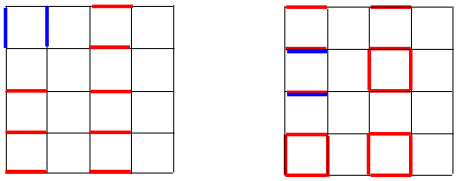

FIG. 21: Local excitations in the dimer (a) and (b) plaquette states. the flipped bonds are denoted as green bonds. Compare with a local density excitation in the TVB in a triangular and Kagome lattice in Fig.11.

of these local excitations through the whole lattice leads to the excitations spectra shown in Fig.24.

Appendix B: Magnetic space group in a honeycomb lattice

In this appendix, we apply the same method in the Section II to study the symmetry breaking insulating states in a honeycomb lattice whose dual lattice is a triangular lattice. We only focus at the $q = 2$ case. We reproduced the dimer state in the Fig.23a achieved in[5]. Unfortunately, the plaquette state in Fig.23b was not identified

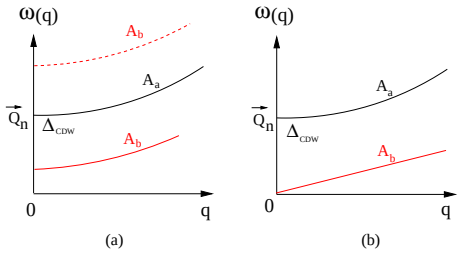

FIG. 22: The excitation spectra in (a) CDW. The lower branch of A_b appears due to the non-zero chemical potential μ in Fig.3a. In the absence of this chemical potential, namely, $\mu = 0$, then the A_b shown as a dashed line is well above the CDW mode A_a. (b) CDW+ SS state.

in[5]. We also work out the excitation spectra in all these insulating states and corresponding supersolid states.

The Harper's equation at $q = 2$ in a honeycomb lattice leads to the vortex field in the Eqn.13 in[5]:

$$\psi(\vec{x}) = e^{i\vec{k}\cdot\vec{x}}\phi_+(\vec{x}) + e^{-i\vec{k}\cdot\vec{x}}\phi_-(\vec{x}) \tag{B1}$$

where $\vec{k} = (\pi/3, \pi/3)$.

In the Ising case $v > 0$: $\phi_+ = 1, \phi_- = 0$, the vortex fields, kinetic energies and currents are shown in Fig.19b. the corresponding excitation spectra are given in the Fig.22.

In the easy plane limit[5] $v < 0$, there are also two cases depending on the signs of the cubic term $w\cos 3\theta$:

(A) If $w > 0$, then $\phi_+ = \phi_- e^{i(2n+1)\pi/3}, n = 0, 1, 2$. The vortex fields, kinetic energies of the $n = 0$ case with $\phi_- = 1$ is shown in Fig.23a. It is a dimer state.

(B) If $w < 0$, then $\phi_+ = \phi_- e^{i2n\pi/3}, n = 0, 1, 2$. The vortex fields, kinetic energies of the $n = 0$ case with $\phi_- = 1$ is shown in Fig.23b. It is plaquette state.

Again, the corresponding local low energy excitations in the dimer and plaquette states in the honeycomb lattice can be similarly constructed as those in the square lattice Fig.21. Because the density remains uniform, so there is no associated density wave excitation. The translational moving of these local excitations through the whole lattice leads to the excitations spectra shown in Fig.22. From Eqn.22 in[5], we can achieve the excitation spectra across the VBS to the VB-SS transition in Fig.24. It is instructive to compare Fig.24 with its counterpart across the CDW to CDW-SS transition Fig.22.

Appendix C: Density operators on square latices

In this appendix, we compare our gauge invariant density operator, kinetic energy and current methods with the density operator formalism developed in[1,21]. We pointed out some potential problems with the density operator formalism in[1,21] and also stress the different conclusions reached by the two methods.

In the dual vortex methods developed in[1], how to characterize the CDW order of bosons on direct lattice in

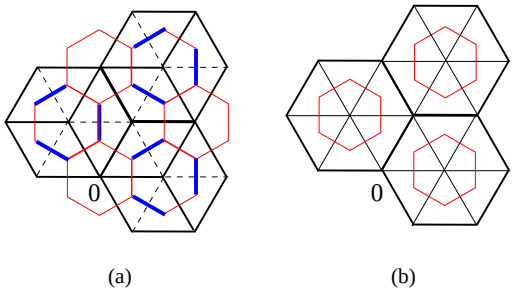

FIG. 23: Easy-plane limit in a honeycomb lattice (a) Dimer state. The dashed line is the frustrated vortex bond with strength $K_f = -1$. The un-frustrated vertical vertex bond is $K = 2$. The blue bond which is perpendicular to the frustrated vortex bond is the boson valence bond in the direct honeycomb lattice. The bosons are hopping along the blue bond. (b) Plaquette state. Because the vortex field vanishes at $(1, 0)$, the kinetic energies emanating from the zero vortex field points are also zero, so there is a local superfluid around this dual lattice point as indicated by the red honeycomb. The bosons are hopping around the red honeycomb. There are no frustrated bonds. All the other bonds have strength $K = 3$. There are no vortex currents in both (a) and (b) indicating no CDW order, so the boson densities are fixed at $f = 1/2$.

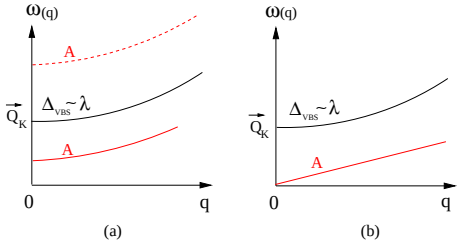

FIG. 24: The excitation spectra in (a) VBS. the VBS gap is given by the operator $w\cos 3\theta$ in Eqn.22 in[5]. The lower branch of A appears due to the non-zero chemical potential μ in Fig.3b in[5]. In the absence of this chemical potential, namely, $\mu = 0$, then the A is well above the VBS mode. (b) VB-SS state.

terms of vortex operators on dual lattice is a little bit tricky. In[1], the density operator parameter was constructed to be the most general gauge invariant bilinear combinations of the vortex fields:

$$\begin{aligned} \tilde{\rho}(\vec{x}) &= \sum_{r,s=-q}^{q-1} \tilde{\rho}_{r,s} e^{i2\pi f(rx+sy)} \\ \tilde{\rho}_{rs} &= S(|\vec{Q}_{rs}|\omega^{-rs/2} \sum_{l=0}^{q-1} \phi_l^* \phi_{l+s} \omega^{-lr} \end{aligned} \tag{C1}$$

where $\vec{Q}_{rs} = 2\pi f(r, s)$ is the ordering wavevector and $S(|\vec{Q}_{rs}|$ is a general form factor which can not be determined from symmetry considerations and depend on the microscopic details. For simplicity without affecting the symmetry of the underlying state, it can be taken as a

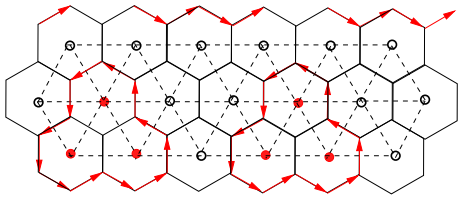

FIG. 25: The possible bubble CDW phase in a triangular lattice in the easy plane limit $v < 0, w > 0$ at $f = 1/3$. By counting the segments of currents along the bonds surrounding hexagons, paying special attentions to their counterclockwise or clock wise directions, we can calculate the densities at the red and black points $n_r = 1/3 + 4xI > 1/3, n_b = 1/3 - 2xI < 1/3$. The $x \sim n_r - n_b > 0$ can be thought as a bubble CDW order parameter and can be tuned by the distance away from the SF to the CDW transition in the Fig.3a. When one tunes the density $n_b = 0$ which stand for vacancies, then $n_r = 1$ which stands for one boson. Note the vortex field at the center of the red loop is non-vanishing, only the current emanating from the center vanish due to the cancelations of currents from neighboring red sites, but the kinetic energies are positive. This indicates a local CDW order.

$\vec{a}_1)\psi(\vec{x}), K_v(\vec{x}) = \psi^*(\vec{x}+\vec{a}_2)e^{i2\pi f a_1}\psi(\vec{x})$:

$$\begin{aligned}
(\rho, K_h, K_v)(\vec{x}) &= \sum_{r,s=0}^{q-1} (\rho_{rs}, K^h_{rs}, K^r_{rs}) e^{i2\pi f(rx+sy)} \\
\rho_{rs} &= A_{rs}[\omega^{-rs} \sum_{l=0}^{q-1} \phi^*_l \phi_{l+s} \omega^{-lr}] \\
A_{rs} &= \frac{1}{N} \sum_{m=0}^{q-1} c^*_m c_{m+r} \omega^{-ms} \\
K^h_{rs} &= A^h_{rs}[\omega^{-rs} \sum_{l=0}^{q-1} \phi^*_l \phi_{l+s} \omega^{-lr}] \\
A^h_{rs} &= \frac{1}{N} \sum_{m=0}^{q-1} c^*_m c_{m+r} \omega^{-m(s+1)} \\
K^v_{rs} &= A^v_{rs}[\omega^{-(r-1)s} \sum_{l=0}^{q-1} \phi^*_l \phi_{l+s} \omega^{-lr}] \\
A^v_{rs} &= \frac{1}{N} \sum_{m=0}^{q-1} c^*_m c_{m+r-1} \omega^{-ms}
\end{aligned} \tag{C2}$$

Lorentzian $S(Q) = \frac{1}{Q^2+1}$. Then Eqn.C1 was evaluated at the direct lattice point, the link points and the dual lattice points to represent the boson density, kinetic energy and the ring exchange amplitudes respectively. As argued in[5], the link points of a square lattice is still a square lattice with a lattice constant $\sqrt{2}$, the dual lattice points of a square lattice is still a square lattice withe same lattice constant. Putting the direct, link and dual lattices together forms a square lattice with a lattice constant $1/2$. This may be the reason why the density operator in Eqn.C1 is the sum from $-q$ to $q-1$ and contains a factor $\omega^{-rs/2}$ which is non-periodic under $f \to f+1$. As pointed out in[5], it is very hard to extend the density operator defined in[1] in square lattice to other lattices. In this appendix, we give a simple way to construct the density and bond operators for any general q in terms of the dual vortex operator and then we will discuss the relations and difference between the two methods.

The q eigenstates $\chi_l; l = 0, 1, \cdots, q-1$ which forms a q dimensional representation of the magnetic space group (MSG) [38] can be written as $\chi_l(\vec{x}) = \frac{1}{\sqrt{N}} \sum_{m=0}^{q-1} c_m \omega^{-ml} e^{i2\pi f(mx+ly)}$ where $\vec{x} = (x, y)$. Then expand the vortex operator $\psi(\vec{x}) = \sum_{l=0}^{q-1} \phi_l(\vec{x})\chi_l(\vec{x})$ where $\phi_l(\vec{x})$ are the q order parameters. Just like Eqns.7,8 in the triangular lattices, one can construct the gauge invariant generalized density operator (GDO) $\rho(\vec{x}) = \psi^*(\vec{x})\psi(\vec{x})$, the bond operators along the horizontal and vertical directions $K_h(\vec{x}) = \psi^*(\vec{x} +$

By construction, all these operators transform like a density, a bond or a current operator and is also periodic under $f \to f+1$. We need evaluate these quantities only at dual lattice points to characterize the CDW and VBS orders in the direct lattice.

Note that gauge invariant physical quantities constructed in Eqns.C2 where the sum is from 0 to $q-1$ and contain only $f \to f+1$ periodic factors such as ω^{-rs}. However, in Eqn.C1, the sum is from $-q$ to $q-1$ and contains a factor $\omega^{-rs/2}$ which is non-periodic under $f \to f+1$. Of course, the original EBHM in Eqn.1 is not periodic under $f \to f+1$, because all the interaction terms do depend on the filling factors f, however, we believe the the symmetry of the insulating states should be periodic under $f \to f+1$. This is what the Eqn.C1 originally designed for: characterize the symmetry breaking patterns of the insulating states only without the ability to spell out the microscopic details. As argued in[5], although Eqn.C1 seems work well in a square lattice and gives the same states shown in the appendix A, but it may not work in a honeycomb lattice. Similar density operators in a triangular were constructed in[21], they gave the same CDW state in the Ising limit $v > 0$ and the stripe CDW state in the easy plane limit $v > 0, w < 0$, but it leads to a bubble CDW state in the easy plane limit $v > 0, w > 0$ in Fig.25 which is completely different than the CDW-VB state shown in Fig.7. This disagreement calls for some re-examinations of the density operators constructed in[1,21]. No such density operators were constructed on honeycomb and Kagome lattices yet.

Appendix D: The vortex fields at a triangular lattice in the easy plane limit $v < 0, w > 0$.

The vortex fields are shown graphically in the Fig.5 and have period 3 along both a_1 and a_2 directions. Their specific values at $\vec{x} = (a_1 = 0, 1, 2, a_2 = 0, 1, 2)$ are listed in the following two 3×3 matrices:

$$\psi_a(\vec{x}) = \begin{pmatrix} 2\sin(\pi/3)\cos(\pi/18)e^{i\pi/9} & 2\sin(\pi/3)\cos(\pi/18)e^{-i4\pi/9} & 0 \\ 2\sin(\pi/3)\cos(\pi/18)e^{i2\pi/9} & 0 & 2\sin(\pi/3)\cos(\pi/18)e^{-i5\pi/9} \\ 3\sin(4\pi/9)e^{i\pi/6} & 2\sin(\pi/3)\cos(\pi/18)e^{-i5\pi/9} & -2\sin(\pi/3)\cos(\pi/18)e^{i\pi/9} \end{pmatrix}$$

$$\psi_b(\vec{x}) = \begin{pmatrix} \sin(\pi/3)e^{-i\pi/6} & -2i\sin(\pi/3)\cos(2\pi/9) & 2\sin(\pi/3)\cos(2\pi/9)e^{i\pi/6} \\ -\sin(\pi/3)e^{i\pi/6} & -\sin(\pi/3)e^{i\pi/6} & 2\cos(2\pi/9)(\sin(\pi/9)+\sin(2\pi/9))e^{i\pi/6} \\ -2i\cos(2\pi/9)(\sin(4\pi/9)+\sin(2\pi/9)) & -2\sin(\pi/3)\cos(2\pi/9)e^{i\pi/6} & 2\cos(2\pi/9)(\sin(4\pi/9)+\sin(2\pi/9))e^{i\pi/6} \end{pmatrix} \quad \text{(D1)}$$

[1] L. Balents, L. Bartosch, A. Burkov, S. Sachdev, and K. Sengupta, Phy. Rev. B **71**, 144508 (2005).
[2] G. Murthy, D. Arovas, and A. Auerbach, Phys. Rev. B **55**, 3104 (1997).
[3] Longhua Jiang and Jinwu Ye, J. Phys. Cond. Matt. **18**, 6907 (2006).
[4] Jinwu Ye, cond-mat/0503113, unpublished.
[5] Jinwu Ye, Nucl. Phys. B **805**, 418 (2008).
[6] D. Jaksch, C. Bruder, J. I. Cirac, C. W. Gardiner, and P. Zoller, Phys. Rev. Lett. **81**, 3108 (1998).
[7] M. Greiner, O. Mandel, T. Esslinger, T. W. Hansch, T. Bloch, Nature **415**, 39 (2002).
[8] G. Grynberg, B. Lounis, P. Verkerk, J.-Y. Courtois, and C. Salomon, Phys. Rev. Lett. **70**, 2249 (1993).
[9] L. Santos, M. A. Baranov, J. I. Cirac, H.-U. Everts , H. Fehrmann1, and M. Lewenstein, Phys. Rev. Lett. **93**, 030601 (2004); B. Damski, H. Fehrmann, H.-U. Everts, M. Baranov, L. Santos, and M. Lewenstein, Phys. Rev. A **72**, 053612 (2005).
[10] A. Griesmaier, J. Werner, S. Hensler, J. Stuhler and T. Pfau, Phys. Rev. Lett. **94**, 160401 (2005)
[11] K.-K. Ni, *et al*, Science **322**, 231 (2008).
[12] B. Capogrosso-Sansone, *et al*, arXiv:0906.2009.
[13] E. Urban *et al*, Nat. Phys, in press; A. Gaetan. *et al*, Nat. Phys. in press. Jan.2009
[14] G. Pupillo, *et al*, arXiv:1001.0519.
[15] K. Baumann, C. Guerlin, F. Brennecke, T. Esslinger, arXiv:0912.3261, to appear in NATURE,
[16] H. P. Bchler, M. Hermele, S. D. Huber, M. P. A. Fisher, and P. Zoller, Phys. Rev. Lett. **95**, 040402 (2005).
[17] R. G. Melko, *et al*, Phys. Rev. Lett. **95**, 127207 (2005).
[18] D. Heidarian and K. Damle, Phys. Rev. Lett. **95**, 127206 (2005).
[19] S. Wessel and M. Troyer, Phys. Rev. Lett. **95**, 127205 (2005).
[20] M. Boninsegni and N. Prokof'ev, Phys. Rev. Lett. **95**, 237204 (2005).
[21] A.A. Burkov and L. Balents, Phys. Rev. B **72**, 134502 (2005).
[22] T. Senthil *et.al*, Science **303**, 1490 (2004).
[23] R. G. Melko, A. Del Maestro, A. A. Burkov, Phys. Rev. B **74**, 214517 (2006).
[24] Jing Yu Gan, Yu Chuan Wen, Jinwu Ye, Tao Li, Shi-Jie Yang, Yue Yu, Phys. Rev. B **75**, 214509 (2007).
[25] K. Sengupta, S. V. Isakov, and Y. B. Kim, Phys. Rev. B **73**, 245103 (2006).
[26] S. V. Isakov, S. Wessel, R. G. Melko, K. Sengupta, and Y. B. Kim, Phys. Rev. Lett. **97**, 147202 (2006).
[27] K. Damle and T. Senthil, Phys. Rev. Lett. **97**, 067202 (2006).
[28] Jinwu Ye, arXiv:0804.3429, unpublished.
[29] Jinwu Ye, Phys. Rev. B **71**, 125314 (2005).
[30] A.A. Burkov and E. Demler, Phys. Rev. Lett. **96**, 180406 (2006).
[31] C. Lannert, M.P.A. Fisher and T. Senthil, Phys. Rev. B **63**, 134510 (2001).
[32] Jinwu Ye and Longhua Jiang, Phys. Rev. Lett. **98**, 236802 (2007); Jinwu Ye, Phys. Rev. Lett. **97**, 236803 (2006); Jinwu Ye, Annals of Physics, **323**, 580 (2008).
[33] Jinwu Ye, J.M. Zhang, W.M. Liu, Keye Zhang, Yan Li, Weiping Zhang, arXiv:1001.3230.
[34] F. Hbert *et.al*, Phys. Rev. B **65**, 014513 (2001).
[35] P. Sengupta, *et.al*, Phys. Rev. Lett. **94**, 207202 (2005).
[36] G. G. Batrouni, F. Hebert, R. T. Scalettar, Phys. Rev. Lett. **97**, 087209 (2006); G.G. Batrouni, F.F. Assaad, R.T. Scalettar, P.J.H. Denteneer, Phys Rev A **72**, 031601(R) (2005).
[37] For a review, see C. Lhuillier and G. Misguich, arXiv:cond-mat/0109146
[38] Jinwu Ye, Phys. Rev. Lett. **97**, 125302 (2006); EPL **82**, 16001 (2008), cond-mat/0603269.
[39] Jinwu Ye, Jour. of Low Temp. Phys: **158**, 882 (2010).